Journal of Engineering and Applied Science

RESEARCH Open Access

New definition for torsional irregularity based on floors rotations of reinforced concrete buildings

Khaled M. Alaa*, Khaled F. El-Kashif and Hamed M. Salem

* Correspondence: eng.khalidalaa@gmail.com
Structural Engineering Department, Cairo University, Giza, Egypt

Abstract

Earthquake investigations confirm that un-symmetric buildings suffer more damage than their symmetric counterparts. Torsional vibrations due to irregularity are one of the main factors which cause damage to buildings. Seismic codes include provisions to consider the torsional vibrations in the design of structures. However, the design of the stiff side elements may be unconservative. In this study, a total of 15 Dual system buildings were analyzed using nonlinear dynamic analysis to propose a new definition for torsional irregularity considering the effects of plan asymmetry on the earthquake response of mid-rise dual system buildings. Based on the analysis results, two new equations were derived using nonlinear regression analysis to check the torsional irregularity and the torsional amplification. Afterward, the proposed torsional irregularity provisions were compared with the torsional irregularity provisions of Europe code (EC-8), Japanese code & ASCE 7-16 code, and the results indicate that the torsional irregularity provisions of all the codes are unconservative. The current investigation proposes new equations to be used in the existing codes for torsional irregularity design considerations to improve the accuracy of the current codes' torsional irregularity provisions.

Keywords: Torsional irregularity, Dual system buildings, Floor rotations, Nonlinear dynamic analysis, Applied element method

Background

Introduction

Earthquake events show that buildings with configuration irregularity are more vulnerable to earthquake damages. For example, many torsionally unbalanced buildings suffered severe damage during the 1985 Michanocan earthquake [1], the 1989 Loma Prieta earthquake [2], the 1994 Northridge earthquake [3], and the 1995 Kobe earthquake [3]. All have indicated the effects of torsional vibrations caused by earthquakes.

The effects of plan asymmetry on the earthquake response of the structures were the subject of many studies (e.g., Bozorgnia and Tso (1986) [4]; Chopra and Goel (1991) [5]). Furthermore, the effects of plan asymmetry on the earthquake response of one-story system structure designed by various codes and how well the torsional provisions

in building codes represent these effects were the subject of many studies (e.g., Chopra and Goel (1991) [6]; Rutenberg (1992) [7]; Wong and Tso (1995) [8]; HUMAR and KUMAR (2000) [9]; HUMAR and KUMAR (2004) [10]).

In 2013, the seismic performance of an under-designed plan-wise irregular R/C structure and different strategies for the seismic retrofitting were studied by Marco and compared by nonlinear dynamic time-history analyses and simplified assessment procedures based on nonlinear static pushover analyses. Numerical results showed that combining the FRP wrapping approach and R/C jacketing applied to the selected columns significantly improved the structure's seismic performance, increasing strength, stiffness, and ductility [11].

In 2014, a parametric investigation was performed by zmen on torsional amplification factor of American Society of Civil Engineers (2010) code (ASCE 7-10) using linear static lateral load analysis; it was found that floor rotations may be considered as the actual representative of the torsional behavior and suggested that torsional irregularity coefficients as defined in the regulations should be amended entirely [12].

In 2018, numerical models were developed by Marco et al. to simulate the seismic response RC frames in the original and retrofitted configurations. First, the effectiveness of three different retrofitting solutions countering the main structural deficiencies of the RC frame is evaluated through the displacement-based approach. Then, nonlinear dynamic analyses are carried out to assess and compare the seismic performance of the RC frame in the original and retrofitted configurations. The combined use of different approaches may represent a valuable tool to accurately address the retrofitting interventions and assess their effectiveness to reduce the seismic vulnerability of poorly designed RC buildings [13].

As the torsional irregularity provisions for the design of stiff side elements in buildings codes may be unconservative, and the stiff element design force could be underpredicted [9], where the stiff side is the side of the unsymmetric structure which the center of rigidity shifted toward it due to asymmetry and the stiff side elements are the elements located in this side as shown in Fig. 1, the current study used nonlinear

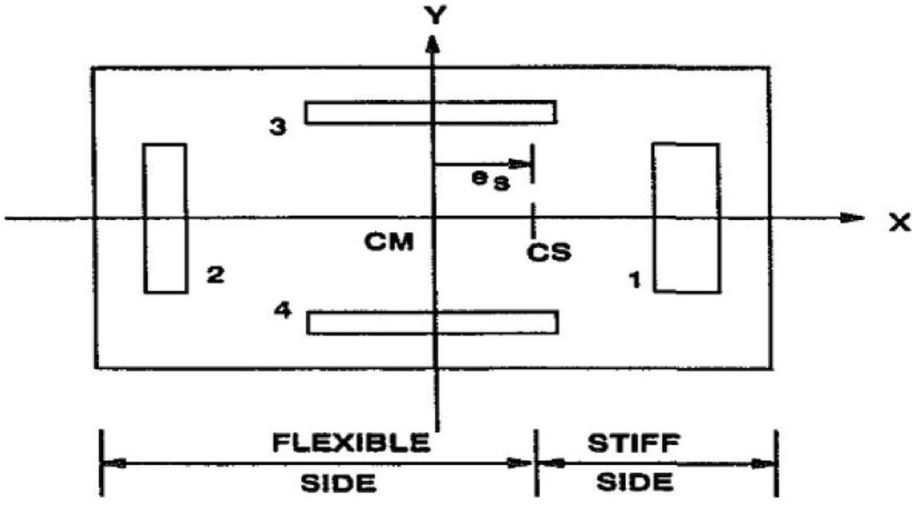

Fig. 1 Stiff side and flexible side elements [5] (stiff side elements: wall (1)/flexible side elements: Wall 2, 3, and 4)

dynamic analysis to propose new equations to be used in the current codes for torsional irregularity design considerations to improve the accuracy of the current codes' torsional irregularity provisions. The new equations are based on the floor rotations, which are the most realistic to represent the torsional behavior of the building.

The main objectives of the study are: Carrying out a parametric study on Dual System structures (D.S.) in terms of eccentricity ratio (distance between the center of mass and center of rigidity normalized by plan dimension) and Peak Ground Acceleration (P.G.A.), propose a new equation to check the torsional irregularity and a new equation for torsional amplification factor (to account for torsional irregularity) based on the rotation of rigid floors by using nonlinear regression analysis and comparing the proposed torsional irregularity provisions with the torsional irregularity provisions of Europe code (EC-8), Japanese code & ASCE 7-16 code.

Code provisions

Code provisions usually include values of static design eccentricities between the center of rigidity and the center of mass. The seismic loads are applied through the design eccentricities points. In some codes, static design or accidental eccentricities are multiplied by factors to account for torsional vibrations such as ASCE 7, U.B.C. 97, NEHRP 199, and N.Z.S. 1992. The design eccentricity formula is shown in Eq. (1) for flexible side elements and Eq. (2) for stiff side elements; values of δ, α, β vary among building codes. Some other codes consider torsional irregularity through modification of seismic reduction factor R, such as Europe code (EC-8) and Japanese code.

$$ed = \alpha \ es + \beta b \tag{1}$$

$$ed = \delta es - \beta b \tag{2}$$

Torsional irregularity provisions of ASCE 7-16/UBC 97

The design eccentricity coefficients specified in ASCE 7-16/UBC97 are α = 1.0, $\beta = A_x$ * (0.05b) and δ = 1.0.

Torsional irregularity and extreme torsional irregularity are defined to consider the maximum story drift and accidental torsion with A_x = 1.0. For torsional irregularity, the ratio between the maximum drift at a story and the average drift of two ends at that story is more than 1.2; this ratio is considered 1.4 for extreme torsional irregularity. If the torsional irregularity exists, the analysis must be performed using accidental torsion amplified by factor A_x. Factor A_x can be considered from Eq. (3) for the torsional irregularity case and Eq. (4) for the extreme torsional irregularity case [14, 15].

$$1.0 \leq \ Ax = \left[\frac{\delta \ \max}{1.2\delta \ \text{avg}}\right]^2 \leq 3.0 \tag{3}$$

$$1.0 \leq \ Ax = \left[\frac{\delta \ \max}{1.4 \ \delta \ \text{avg.}}\right]^2 \leq 3.0 \tag{4}$$

Torsional irregularity provisions of Japanese code

Japanese code considers torsional irregularity through modification of seismic reduction factor R by multiplying the seismic reduction factor by the basic shape factor F_e.

Torsional irregularity is defined to exist where the eccentricity factor R_e exceeds 0.15. Factor R_e is determined from the following equation [16].

$$R_{ex} = \frac{ey}{\sqrt{\frac{lx+ly}{\Sigma Kx}}}, R_{ey} = \frac{ex}{\sqrt{\frac{lx+ly}{\Sigma Ky}}} \tag{5}$$

In case R_e exceeds 0.15, the ultimate lateral shear strength of each story Q_{ud} must be calculated, and it must be confirmed to be not less than the specified ultimate shear as decreased by the factor F_e. Then, the specified ultimate shear Q_{un} is determined by Eq. (6) [16].

$$\text{Specified ultimate shear } Q_{un} = R{*}F_e{*}Q_{ud} \tag{6}$$

The basic shape factor F_e is determined from Table 1.

Torsional irregularity provisions of E.C.-8

Europe code considers torsional irregularity through reduction of seismic reduction factor R. Frame, dual or wall systems classified as torsionally flexible systems, if at any floor one or both of the following equations not met [17].

$$rx \geq ls = \sqrt{\frac{\text{torsional stiffness}}{\text{lateral stiffness}-y \text{ direction}}} \geq \sqrt{\frac{(L^2+b^2)}{12}} \tag{7}$$

$$ry \geq ls = \sqrt{\frac{\text{torsional stiffness}}{\text{lateral stiffness}-x \text{ direction}}} \geq \sqrt{\frac{(L^2+b^2)}{12}} \tag{8}$$

If the system is classified as a torsionally flexible system, the basic value of the seismic reduction factor R is reduced to a value of R = 2 for ductility class medium (D.C.M.) or R = 3 for ductility class high (D.C.H.) as shown in Table 2. Basic values of the seismic reduction factor R for systems regular in elevation are shown in Table 2 [17].

Analysis methods

The applied element method, AEM, was developed by Tagel-Din and Meguro, 1999 [18]. The main advantage of this method is that it can follow the structural behavior from the application of load to the total collapse of the structure with high accuracy and reasonable time. In addition, the crack opening and crack closure process can be followed [18].

The structure is modeled as an assembly of small elements made by virtually dividing the structure, as shown in Fig. 2a. The elements are assumed to be connected by normal and shear springs, as shown in Fig. 2b, representing the stress and deformation of a specific area [hatched area in Fig. 2b] [19]. For example, the matrix springs and reinforcement springs represent concrete and reinforcing steel bars in reinforced

Table 1 basic shape factor F_e [16]

R_e	F_e
Re ≤ 0.15	1
0.15 < R_e < 0.3	1/ [1+$\frac{0.5}{0.15}$ (Re–0.15)]
0.3 ≤ Re	1/1.5

Table 2 Basic values of the seismic reduction factor, *R*, for systems regular in elevation [17]

Structural type	DCM	DCH
Frame system, dual system, coupled wall system	3.0(a_u/a_1)	4.5(a_u/a_1)
Uncoupled wall system	3.0	4.0(a_u/a_1)
Torsionally flexible system	2.0	3.0
Inverted pendulum system	1.5	2.0

concrete structures, as shown in Figs. 3 and 4 [20]. The stiffness matrix is formulated by applying unit displacements in the six degrees of freedom for each element, calculating the forces generated in the springs, and calculating the element forces in the directions of the degrees of freedom, as illustrated in Fig. 5 [20].

For modeling of concrete under compression, the compression model of Maekawa [21] shown in Fig. 6a is adopted in Extreme Loading for Structures (ELS) [20]. For concrete springs subjected to tension, spring stiffness is assumed as the initial stiffness until the spring reaches the cracking point. The stiffness of springs subjected to tension is set to a minimum value after cracking. In the next loading step, the residual stresses are then redistributed by applying the redistributed force values in the reverse direction. The relationship between shear stress and shear strain is assumed to remain linear till the cracking of concrete. Concrete is considered cracked when concrete stresses reach the strength limit. Both normal and shear stresses drop to zero for tensioned concrete.

However, for compressed concrete, the shear stress value is limited to a specific value depending on the compressive stresses, and the shear stress-shear strain relationship follows the curve shown in Fig. 6b. The aggregate interlock and friction at the crack surface control the drop level of shear stresses. This drop is defined as the residual shear strength factor or redistributed value (R.V.). The scheme for the envelope curve steel in tension and compression is shown in Fig. 7a for reinforcement springs. Three stages are considered; elastic, yield plateau, and strain hardening [20]. According to Giuffre and Pinto (1970), which was later implemented in Menengotto and Pinto (1973) [23], unloading and reloading stress-strain models are adopted in the analytical procedures as illustrated in Fig. 7b [20].

In ELS, the nonlinear response stage of RC structures, internal damping can arise due to concrete cracking, energy dissipation due to the loading and unloading of

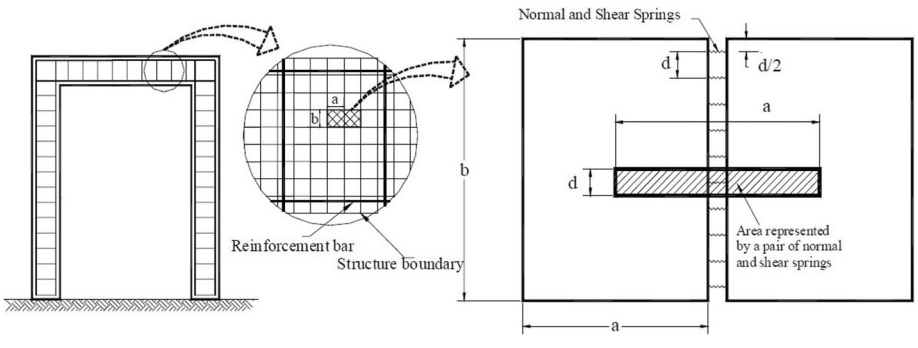

Fig. 2 Modelling of structure in the AEM [19]. **a** Element generation for AEM. **b** Spring distribution and area of influence of each pair of springs

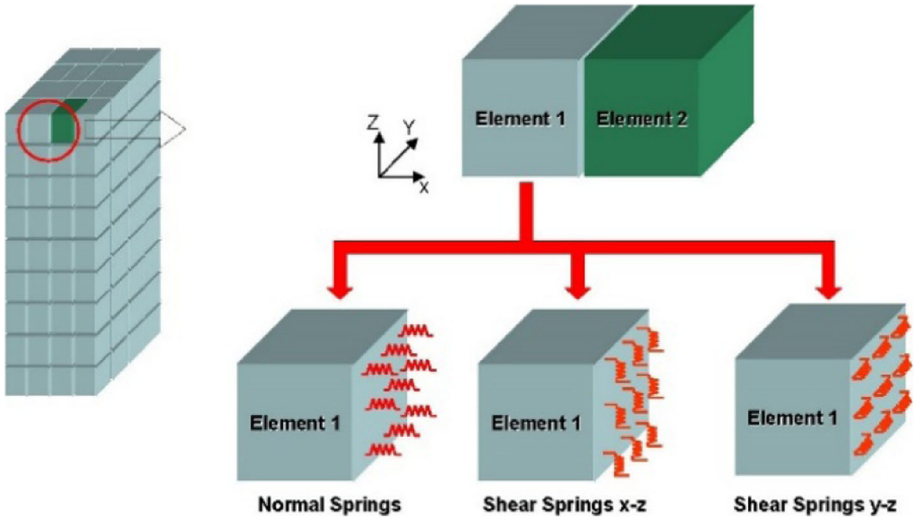

Fig. 3 Matrix springs [20] (color should be used for this figure)

compression springs, unloading of reinforcement after yielding, and friction between elements and unloading factors during contact.

Many studies have been done using the applied element method (e.g., Karbassi and Nollet [24]; Malomo et al. [25]; Sediek et al. [26]).

Structural models

Since the primary purpose of the torsional amplification factor is to limit the additional ductility demand on the stiff-edge element of the un-symmetric system to an acceptable level and as per the Literature Review, the floor rotations may be considered as the actual representative of the torsional behavior, the ductility demand ratio and rotations of buildings are the main parameters in the study. In the parametric study, the effect of earthquake acceleration (a_g), configuration of walls and frames, and distance between

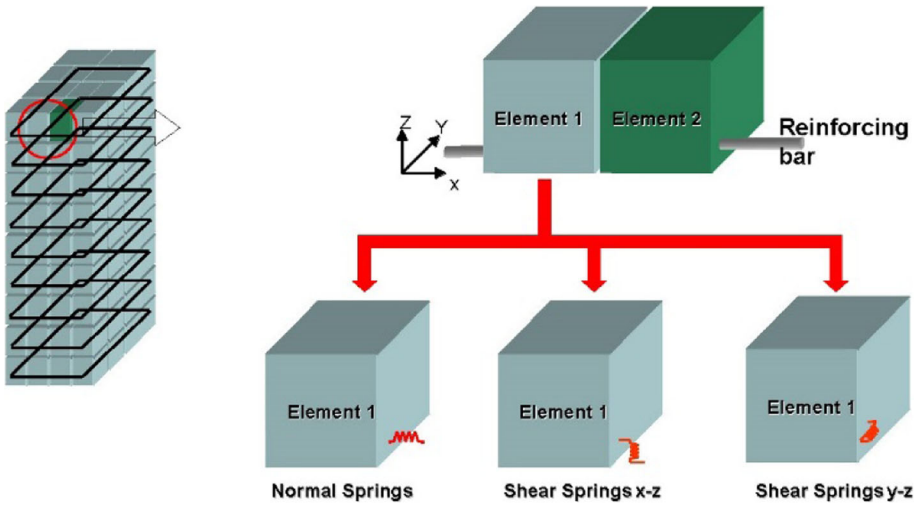

Fig. 4 Reinforcement springs [20] (color should be used for this figure)

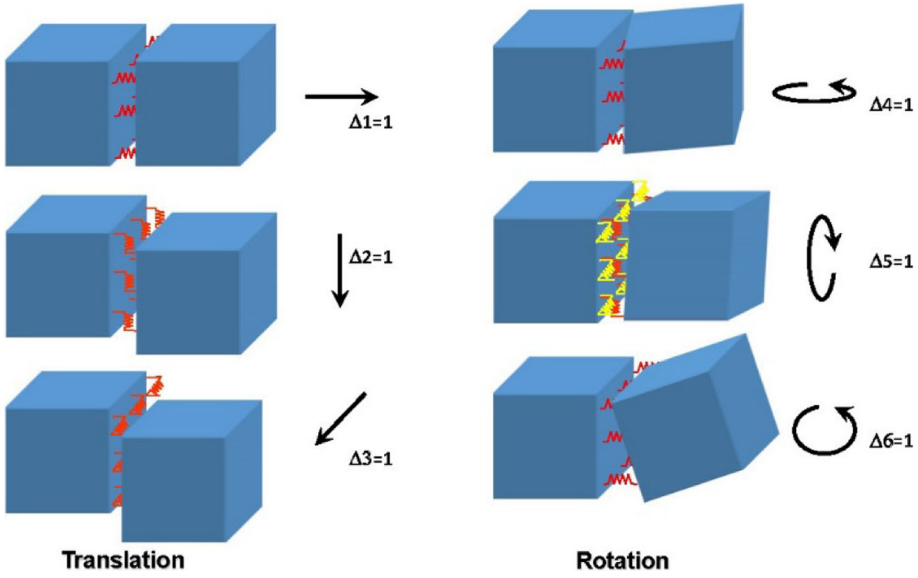

Fig. 5 Formulation of stiffness matrix [20] (color should be used for this figure)

the center of mass and the center of rigidity normalized by plan dimension (es/b) on rotation and ductility demand ratio were considered. The study is performed on three groups, where each group represents varying (es/b) with a constant (a_g) value, and each group consists of four cases. The inelastic responses of a torsionally unbalanced system were normalized to those of a reference model, which is a torsionally balanced model its center of mass coincides with its center of rigidity, to study the effect of torsion, in this parametric study case 4 in each group is the reference model for all groups. Figure 8 shows the general layout of the reference building model. The parameters of studied cases are shown in Table 3.

The studied structures are typical 12-story reinforced concrete buildings with dual systems consisting of intermediate moment frames and ordinary shear walls. The structures are eight and five bays in x- and y-directions, respectively, with bay lengths equal to four meters in both directions. The story height is three meters. The columns are fixed at their base. First, the linear finite element program ETABS [27] has been chosen

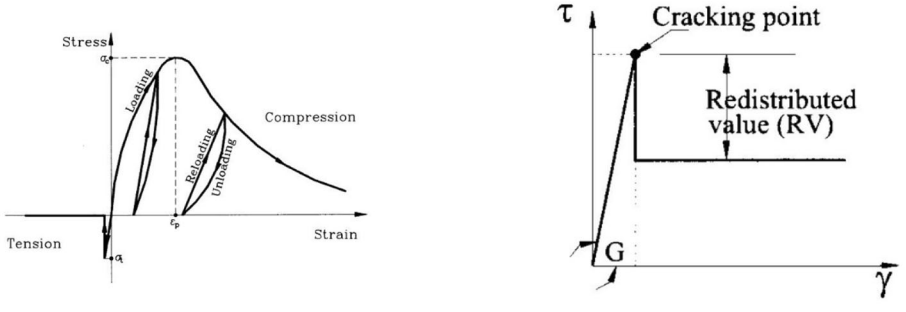

(a) Concrete under axial stresses [20] (b) Concrete under shear stresses [22]

Fig. 6 Constitutive models for concrete used in ELS. **a** Concrete under axial stresses [21]. **b** Concrete under shear stresses [22]

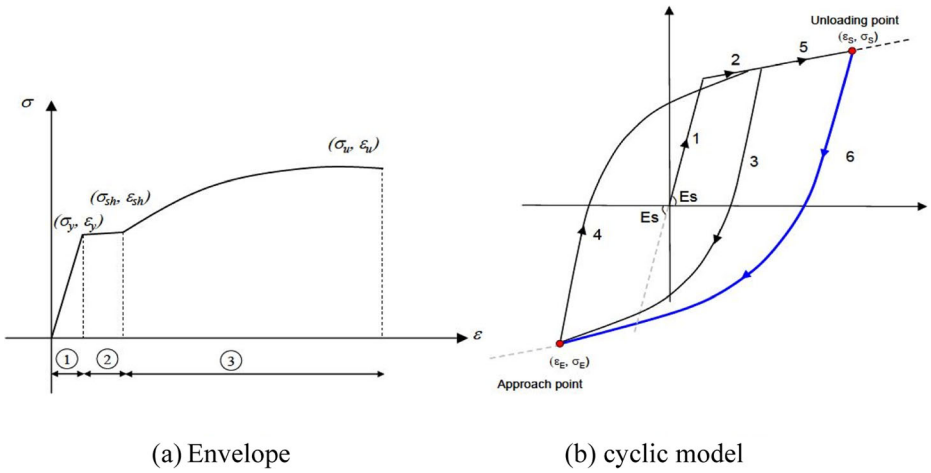

Fig. 7 Constitutive models for Reinforcement used in ELS [20]. **a** Envelope. **b** Cyclic model

for the model and the preliminary design of the studied cases. Then, nonlinear time history analysis was performed using applied element method software (ELS) [20].

Gravity and seismic loads

The structure was designed according to American codes (ACI-318-14 [28] and ASCE 7-16 [14]) using the Etabs program. The superimposed dead load is 2.0 kN/m^2 , equivalent uniform wall load is 2.5 kN/m^2 and live loads is 2.0 kN/m^2, respectively. Seismic parameters used in the analysis and design of typical structures are: seismic design category (*C*), soil class (*D*), importance factor = 1.25, response modification factor (*R*) = 5.5, design earthquake spectral response acceleration parameter at short period (S_{DS}) = 0.4166, design earthquake spectral response acceleration parameter at 1-s period (S_{D1}) = 0.0544.

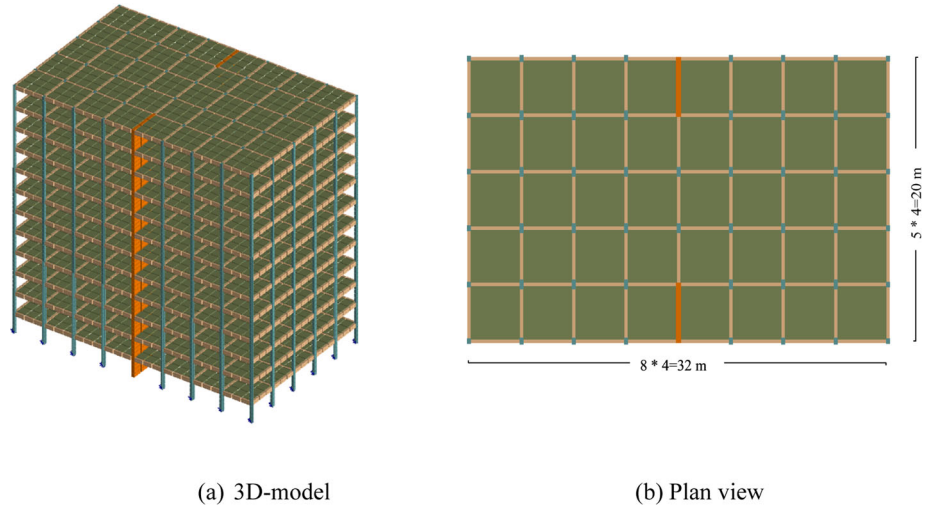

Fig. 8 General layout of the references building model (color should be used for this figure). **a** 3D-model. **b** Plan view

Table 3 Varied parameters of studied cases

Groups	Cases	Ground acceleration (a_g)	(*es*/*b*) (eccentricity normalized by plan dimension perpendicular to the direction of loading)
Group-1	DS-1-1	0.3 g	0.375
	DS-1-2	0.3 g	0.25
	DS-1-3	0.3 g	0.125
	DS-1-4	0.3 g	0
Group-2	DS-2-1	0.45 g	0.375
	DS-2-2	0.45 g	0.25
	DS-2-3	0.45 g	0.125
	DS-2-4	0.45 g	0
Group-3	DS-3-1	0.6 g	0.375
	DS-3-2	0.6 g	0.25
	DS-3-3	0.6 g	0.125
	DS-3-4	0.6 g	0

Time history records

Seismic input to the dynamic analysis of structures is defined in terms of acceleration time series (time-history function) whose response spectra are compatible with a specified target response spectrum with Peak Ground Accelerations (P.G.A.) of 0.3 g, 0.45 g, and 0.6 g. SeismoArtif [29] program has been used to modify a reference time series so that its response spectrum is compatible with a specified target spectrum using the Real Accelerogram Adjustment calculation method. In the Real Accelerogram Adjustment calculation method, the artificial accelerogram is defined starting from a real one and adapting its frequency content to match the target spectrum using the Fourier Transformation Method as shown in Fig. 9 [29].For example, the real accelerogram of the Kobe earthquake shown in Fig. 10, and a response spectrum generated according to ASCE 7-16 shown in Fig. 11 were used to generate our artificial earthquake shown in Fig. 12. Then, the induced artificial earthquake was scaled so that its peak ground acceleration (P.G.A.) matches the P.G.A. of 0.3 g, 0.45 g, and 0.6 g, and these functions were then imported to Etabs and ELS programs to represent the ground motions. The ground motions after the scaling process are shown in Figs. 13, 14, and 15.

Dimension, reinforcement detailing, and material properties

The slab thickness used for a solid slab system was 160 mm with bays of dimensions 4.0 m by 4.0 m. The beams and columns were designed to represent an intermediate moment frame. All the beams are 250 * 600 mm with top reinforcement of 3Ø20 and bottom reinforcement of 3Ø16. Columns dimensions and reinforcement details are

shown in Fig. 16 and Table 4. The characteristics of reinforced concrete are summarized in Table 5, and the characteristics of steel reinforcement are summarized in Table 6. All the walls are 400 mm in width with longitudinal reinforcement of Ø16@150 mm and horizontal reinforcement of Ø14@150 mm.

Calculation of ductility demand ratios and floor rotations

Determination of ductility demand ratios using nonlinear time history analysis In the nonlinear time-history dynamic analysis of structures responding to an earthquake in the inelastic range, the maximum deformations are expressed in Eq. 20. The ductility factor (μ) is the ratio between maximum roof deformation and the corresponding roof deformation present when yielding occurs. The maximum deformations are permitted to be expressed in nondimensional terms as indices of inelastic deformation for seismic design and analysis using ductility factors [30].

$$\mu = \frac{\Delta_{\max}}{\Delta_{\text{yield}}} \tag{20}$$

The definition of yield deformation often causes difficulty when calculating ductility factors since the force-deformation relation may not have a well-defined yield point. Therefore, various definitions for yield deformations have been proposed: deformation corresponding to the first yield as shown in Fig. 17a or deformation corresponding to the yield point of an equivalent elasto-plastic system with the same elastic stiffness and ultimate load as the real system as shown in Fig. 17b or deformation corresponding to the yield point of an equivalent elasto-plastic system with the same energy absorption as the real system as shown in Fig. 17c or deformation corresponding to the yield point of an equivalent elasto-plastic system with reduced stiffness computed as the secant stiffness at 75% of the ultimate lateral load of the real system as shown Fig. 17d [30]. In this study, yield displacement is considered the deformation corresponding to the first yield. For maximum deformation definition, various definitions have been proposed: deformation corresponding to a limiting value of strain as shown in Fig. 18a or deformation corresponding to the apex of the load-displacement relationship as shown in Fig. 18b or deformation corresponding to the post-peak displacement when the load-carrying capacity has undergone a small reduction as shown in Fig. 18c or deformation corresponding to fracture or buckling as shown in Fig. 18d [30]. In this study, the

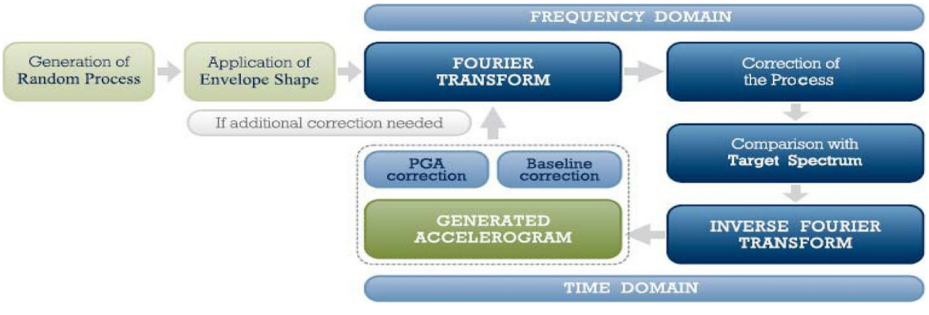

Fig. 9 Real accelerogram adjustment calculation schematic [30]

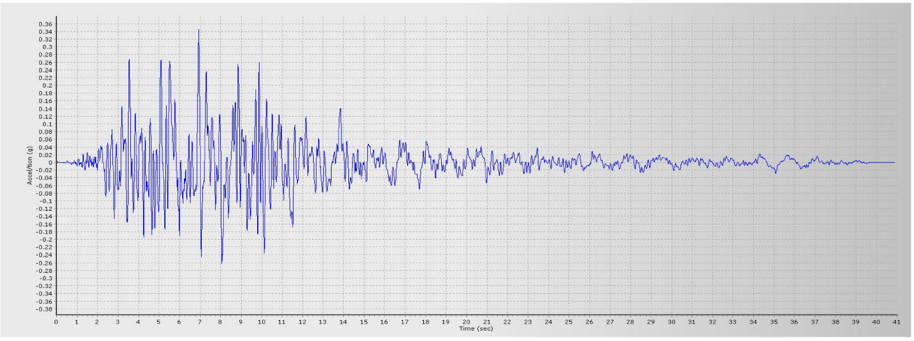

Fig. 10 Real accelerogram (Kobe, Japan, 1995)

maximum displacement is considered the deformation corresponding to the apex of the time-displacement relationship.

In the ELS program, to get the time of the first yielding point, the stresses in RFT bars of beams, walls, and columns were tracked with time; an example of the program output is shown in Figs. 19, 20, and 21. When stress in steel bars springs reaches the yield, the time corresponding to the yield point from Fig. 19 is used. The yield displacement and the displacement corresponding to the time of the first yielding point are calculated as shown in Fig. 20. Maximum (ultimate) deformation is deformation corresponding to the apex of the time-displacement relationship, as shown in Fig. 21. The ductility Demand factor Ratio was calculated by dividing the ductility demand factor of the desired plan- asymmetric plan—by ductility demand factor of reference plan-symmetric plan—in the same group.

Determination of rigid floor rotation using nonlinear time history analysis In the ELS program, floor rotations were tracked with time and rotation corresponding to the apex of a time-rotation relationship considered to be the floor rotations used in the study, as shown in Fig. 22.

Results

Effect of distance between the center of mass and center of rigidity on rotation

The effect of distance between the center of mass and center of rigidity normalized by plan dimension (es/b) on floor rotations using nonlinear dynamic analysis is shown in Figs. 23, 24, and 25. The results show that floor rotations increase as the distance

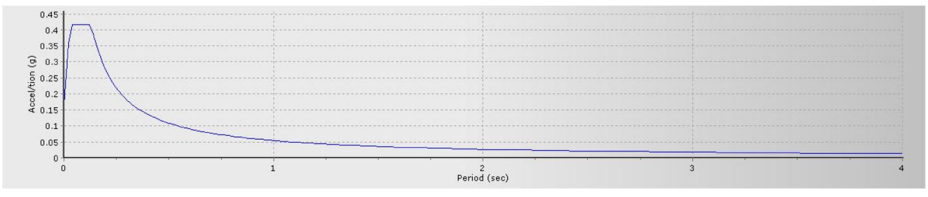

Fig. 11 Target response spectrum of soil class (*D*) and seismic design category (*C*), which generated according to ASCE 7-16

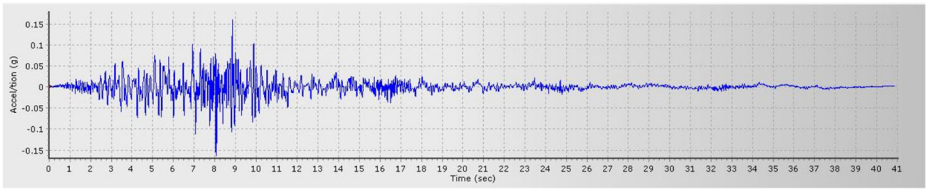

Fig. 12 Artificial accelerogram

between the center of mass and rigidity increases. Furthermore, floor rotations reach their maximum values as the distance between the center of mass and walls increases.

Effect of distance between the center of mass and center of rigidity on ductility demand

Stiff side elements located at 8 m, 12 m, and 16 m from the center of mass were considered in this study to study the effect of distance between the center of mass and center of rigidity on the Ductility demand of stiff side elements. The results of stiff side elements located at 16 m from the center of mass are shown in Figs. 26, 27, and 28. The results show that as the distance between the center of mass and center of rigidity rotation increases, floor rotations increase, and ductility demand ratios increase.

Effect of increasing P.G.A. on floor rotations

The effect of increasing P.G.A. on floor rotations using $^{\text{nonlinear dynamic}}$ analysis is shown in Figs. 29, 30, and 31. The results show that floor rotations increase as Peak ground acceleration (P.G.A.) increases.

Effect of floor number on floor rotation

The effect of floor number on floor rotations using $^{\text{nonlinear dynamic}}$ analysis is shown in Figs. 32, 33, and 34. The results show that as floor number increases, the story rotation increases, maximum floor rotation occurs at the highest stories, maximum rotation at the 12th story.

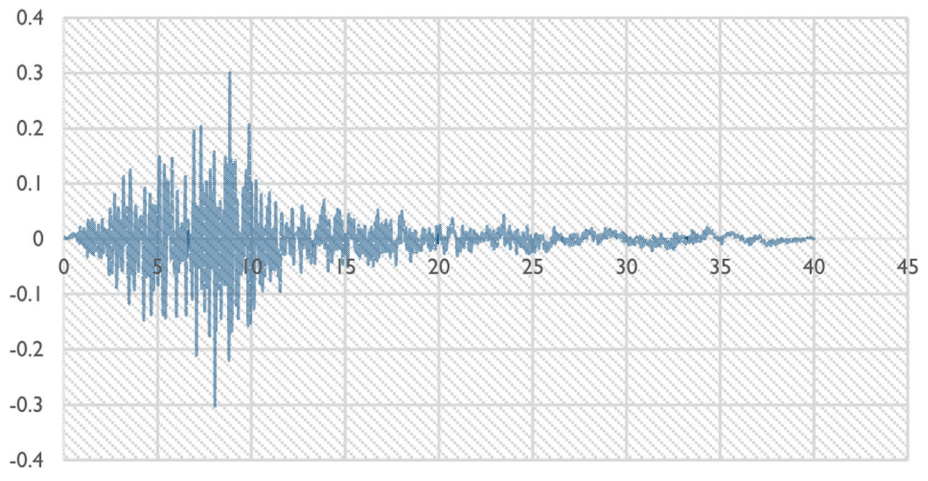

Fig. 13 Scaled artificial accelerogram (P.G.A. = 0.30 g)

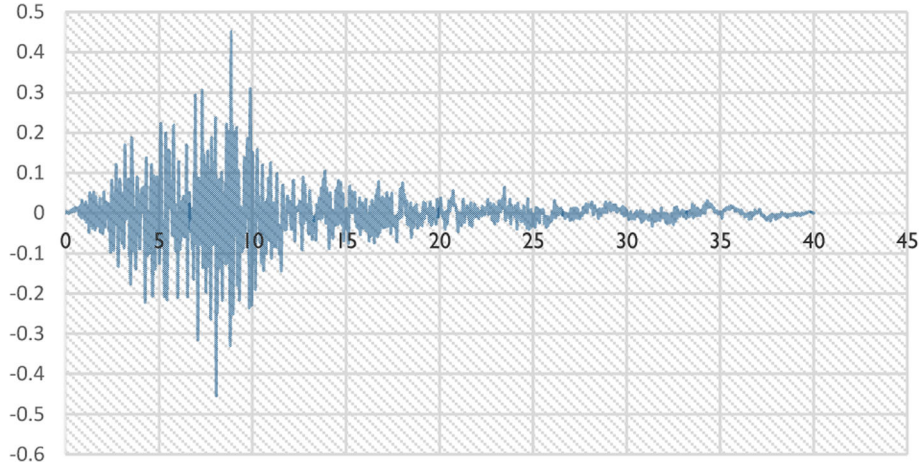

Fig. 14 Scaled artificial accelerogram (P.G.A. = 0.45 g)

Discussion

Upper limit

One of the goals of this research is to derive a simplified equation to check where the torsional irregularity exists based on the rotation of buildings. The proposed equation is derived by using nonlinear regression analysis.

First, separate equations are derived for each group based on floor rotations and ratios of stiff side elements ductility demand located at 8 m, 12 m, and 16 m from the center of mass. To suppose a conservative equation, the best-fit equation of 1st Floor with 0.6 g acceleration of stiff elements with a distance of 16 m from the center of mass used as the base case equation ("U^{θ}_{o}"), as shown in Fig. 35.

Then, the effect of the varying floor no. (2nd, 3rd, 4th, etc.) and varying P.G.A. considered by U_f equation and U_g respectively. Since the derived equation is based on the ductility demand ratio (unsymmetric plan/symmetric plan) and the torsional

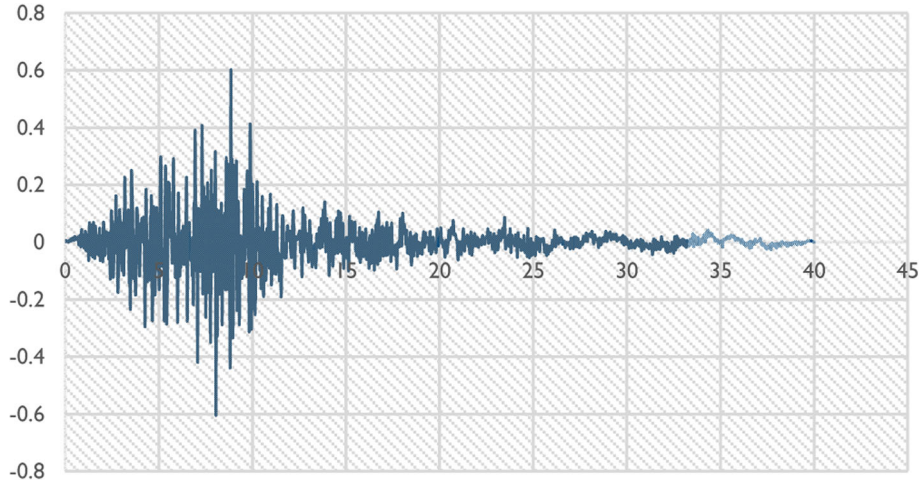

Fig. 15 Scaled artificial accelerogram (P.G.A. = 0.60 g)

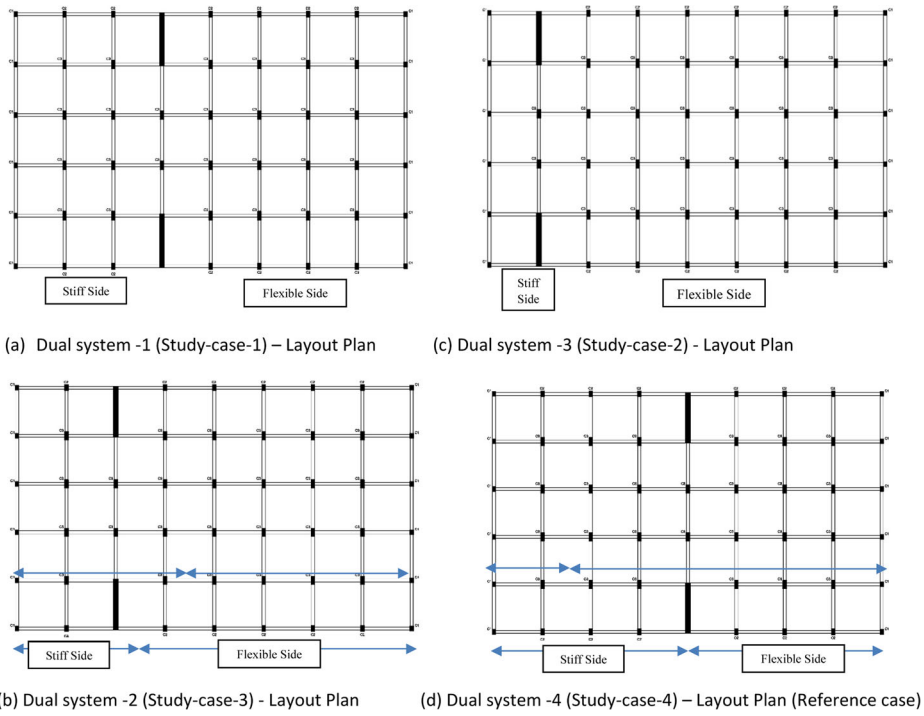

Fig. 16 Study—cases reinforcement plans. **a** Dual system-1 (study-case-1) — layout plan. **b** (b) Dual system-2 (study-case-3) — layout plan. **c** Dual system-3 (study-case-2) — layout plan. **d** Dual system-4 (study-case-4) — layout plan (Reference case)

irregularity is defined to exist where ductility demand ratio larger than 1, the derived equation as shown in Eq. (9) has an upper limit of 1.

$$U = \frac{U^{\theta}_{o}}{U_f * U_g} \leq 1 \tag{9}$$

To consider varying floor no. (2nd,3rd, 4th, etc.), the relation between floor number and U_{Θ} established as shown in Fig. 36, and then, regression analysis used to estimate the equation of U_f, as shown in Eq. (10).

Table 4 Column schedule

MARK	From Foundation level up to under site of 4th slab		From the 4th floor slab to under site of 8th slab		From the 8th floor slab to under site of 12th slab	
C1	Column Size 300 x 400 Vertical Bars 8 T 16 Ties Ø10 @200		Column Size 300 X 400 Vertical Bars 6 T 16 Ties Ø10 @200		Column Size 300 X 300 Vertical Bars 6 T 16 Ties Ø10 @200	
C2	Column Size 300 X 500 Vertical Bars 10 T 16 Ties Ø10 @200		Column Size 300 x 400 Vertical Bars 8 T 16 Ties Ø10 @200		Column Size 300 X 300 Vertical Bars 6 T 16 Ties Ø10 @200	
C3	Column Size 300 X 700 Vertical Bars 16 T 16 Ties Ø10 @200	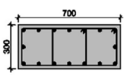	Column Size 300 X 600 Vertical Bars 12 T 16 Ties Ø10 @200	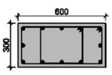	Column Size 300 X 500 Vertical Bars 8 T 16 Ties Ø10 @200	

Table 5 Reinforcement steel properties

Concrete properties	
Young's modulus MPA	25,742.96 MPA
Cylinder compressive strength (fc')	30 MPA
Tensile strength	3.392 MPA
Specific weight (ϒc)	25 kN/m^3
Shear strength	10.95 MPA

$$\mathrm{Uf} = 1.8{*}\mathrm{n}{-}1.04 \tag{10}$$

To consider varying Peak Ground Acceleration (P.G.A.), the relation between P.G.A. and $\frac{U_\theta}{U_f}$ established as shown in Fig. 37, then, regression analysis was used to estimate the equation of $\boldsymbol{U_g}$ **,** as shown in Eq. (11).

$$U_g = 1.7{*}a_g{}^{1.1} \tag{11}$$

By using substitution, the equation of torsional irregularity upper limit Eq. (9) can be written in the form of the following equation:

$$U = \frac{161.7{*}\Theta - 0.2}{(1.8{*}\mathrm{n} - 1.04){*}(1.7{*}\mathrm{ag}\ 1.1)} \leq 1 \tag{12}$$

Torsional amplification factor

One of the goals of this research is to derive a simplified equation for the torsional irregularity coefficient, torsional amplification factor, based on the rotation of buildings. The proposed equation is derived by using nonlinear regression analysis.

Since the main objective of the torsional amplification factor is to amplify the accidental eccentricity for torsionally flexible structural systems and modify the design eccentricity of stiff side elements to account for torsional irregularity effects, therefore, separate equations are derived for each group based on floor rotation – Structural eccentricity normalized by plan dimension (*es*/*b*) relationships. To suppose a conservative equation, the best-fit equation of 1st floor with 0.3 g acceleration used as the base case equation ("$\boldsymbol{e_d}^{o}$"), as shown in Fig. 38.

The effect of the varying floor no. (2^{nd},3^{rd}, 4^{th}, etc.) and varying P.G.A. considered by $\boldsymbol{e_f}$ equation and e_g respectively. Finally, the equation is divided by accidental eccentricity and added to 1 to amplify the accidental eccentricity (0.05), as shown in the following equation.

Table 6 Concrete properties

Reinforcement steel properties	
Young's modulus	20,3890 MPA
Yield strength	400 MPA
Ultimate strength	600 MPA

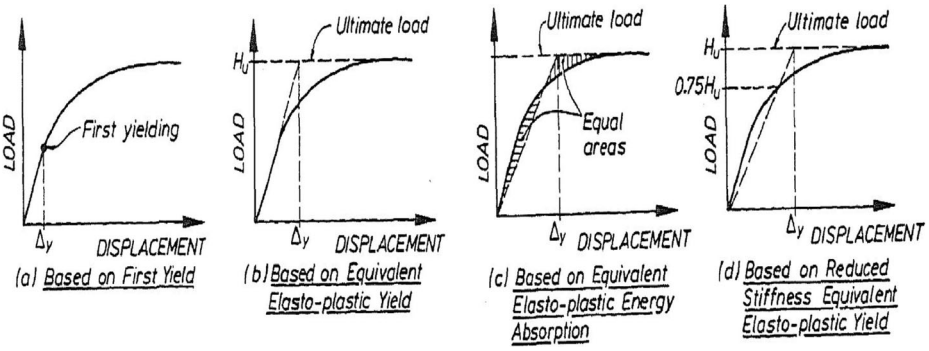

Fig. 17 Alternative definition for yield displacement [30]

$$Ax = 1 + \frac{{e_d}^o}{0.05 * e_f * e_g} \tag{13}$$

To consider varying floor no. (2nd,3rd, 4th, etc.), the relation between Floor number and e_d was established for Group-1 as shown in Fig. 39, and then regression analysis was used to estimate the equation of e_f, as shown in Eq. (14).

$$e_f = 2.02 * n - 1.45 \tag{14}$$

To consider varying Peak Ground Acceleration (P.G.A.), the relation between P.G.A. and $\frac{e_d}{e_f}$ established as shown in Fig. 40, then, regression analysis used to estimate the equation of $\boldsymbol{e_g}$, as shown in Eq. (15).

$$e_g = 1.9 \ ag^{0.55} \tag{15}$$

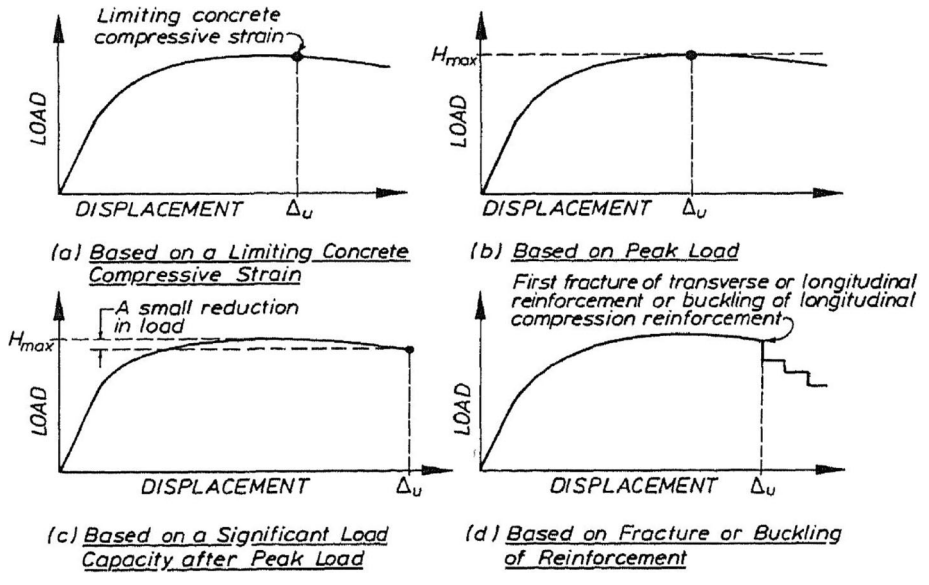

Fig. 18 Alternative definition for ultimate displacement [30]

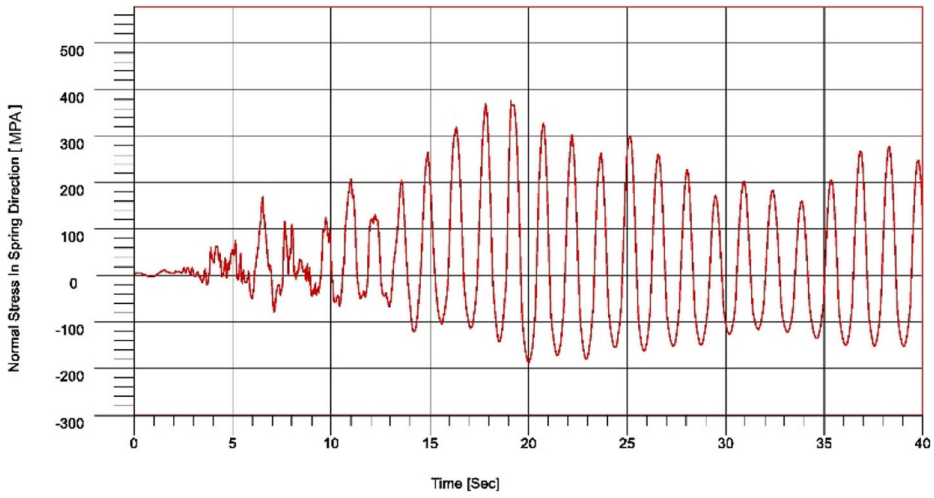

Fig. 19 Beam stress time history (first yielding point)

By using substitution, the equation of torsional amplification factor (Eq. (13)) can be written in the form of the following equation:

$$Ax = 1 + \frac{(20.2 * \Theta - 0.02)}{0.05 * (2.02 * n - 1.45) * (1.9 * \mathrm{ag}\ 0.55)} \tag{16}$$

Comparing systems designed considering torsional irregularity of various codes and the derived equations

Two groups of buildings have been chosen to compare the torsional provisions of ASCE 7-16, E.C.-8, and Japanese code with the derived equation.

First group of buildings

The first group consists of five buildings, as shown in Fig. 41. The five buildings have different eccentricity ratios. The buildings are 12-story in height, and the floor height is

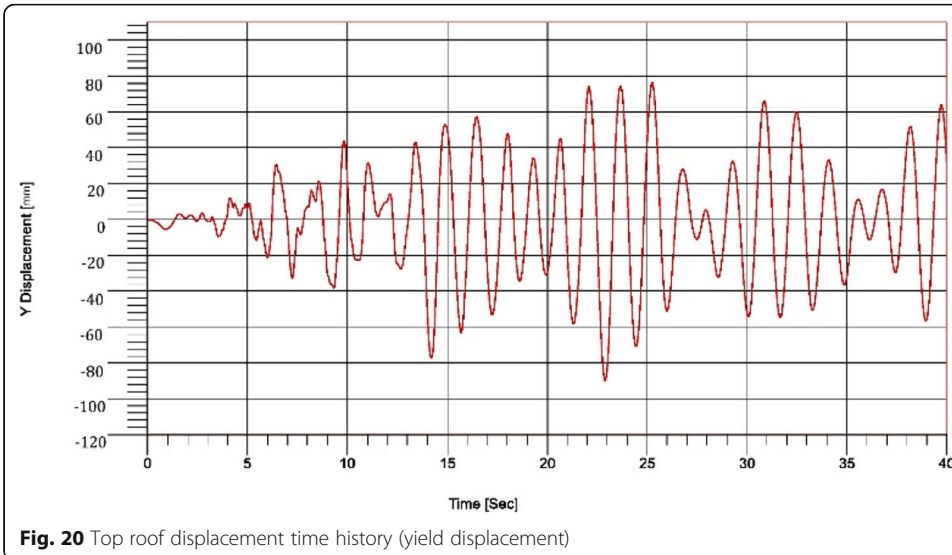

Fig. 20 Top roof displacement time history (yield displacement)

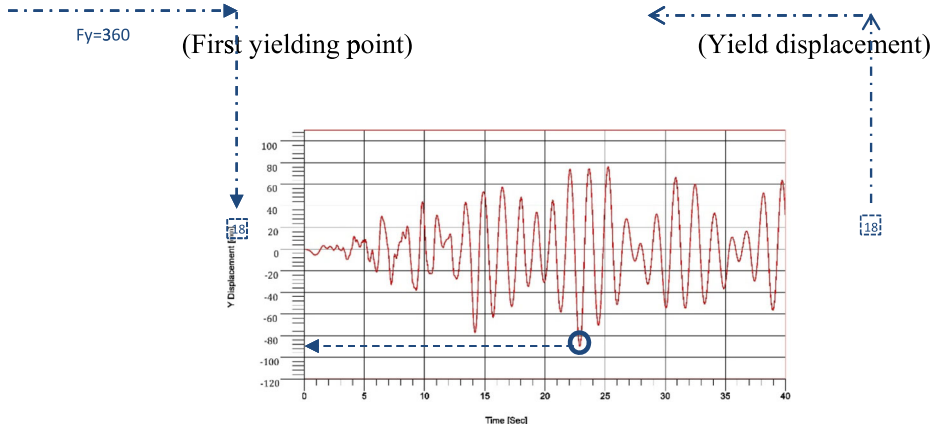

Fig. 21 Top roof displacement time history (maximum displacement)

3 m. The buildings have ten bays in *X*-direction and five in *Y*-direction. The building's structural system is a Dual system with intermediate moment frames and ordinary shear walls. Corner and edge columns are 300 * 900 mm, and all the other inner columns are 300 * 1000 mm, beams size is 300 * 800 mm, wall length is 4 m, and the slab thickness is 160 mm. The columns are fixed at their base. The buildings were studied in Y-direction only.

First, the dimensions of the structural elements were determined by a preliminary design process using the equivalent static seismic load of ASCE 7-16. Second, the torsional irregularity was checked using various codes and the derived equations for all models, as shown in Tables 7, 8, and 9. Third, the torsional irregularity provisions of various codes and the derived equations were considered in the analysis. Fourth, the design forces of resisting elements of the asymmetric building corresponding to those of symmetric building compared as shown in Figs. 42 and 43. Finally, the torsional amplification factor (A_x) of ASCE 7-16 and the derived equation are compared in Fig. 44.

Comparing the design forces of resisting elements of the stiff side elements show that by neglecting the torsional irregularity provisions, there is a reduction in the design force up to 41% for small eccentricity ratios and up to 50% for large eccentricity ratios.

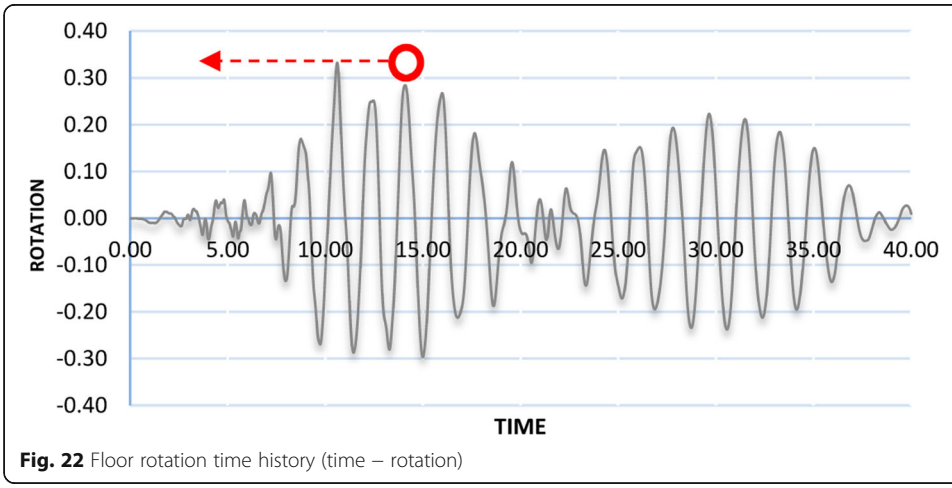

Fig. 22 Floor rotation time history (time – rotation)

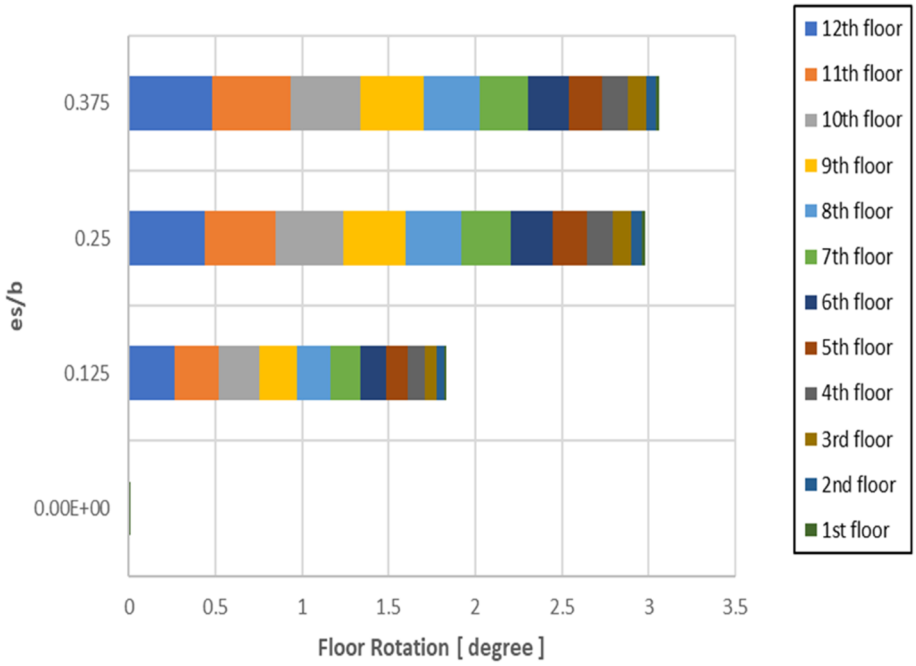

Fig. 23 Comparison of *es/b* — floor rotations for DS-1-1, DS-1-2, D1-1-3, and DS-1-4 (color should be used for this figure)

On the other hand, for the EC-8 code, there is no reduction in the design force ratio of stiff side elements for small eccentricity ratios and up to 6% for large eccentricity ratios. For ASCE 7-16, there is a reduction in the design force ratio of stiff side elements up to 27% for small eccentricity ratios and up to 44% for large eccentricity ratios. For Japanese code, there is a reduction in the design force ratio of stiff side elements up to 41%

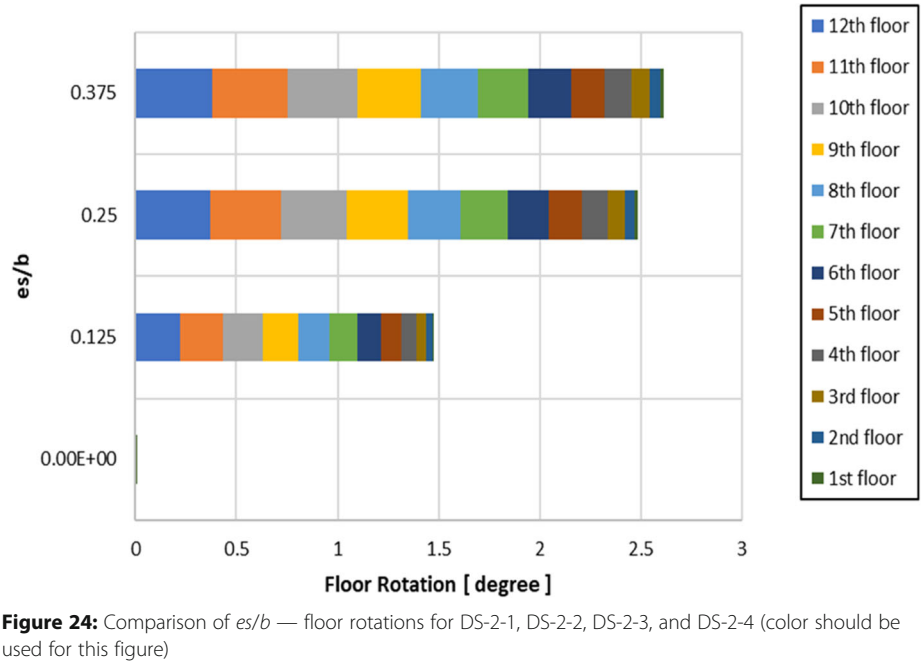

Figure 24: Comparison of *es/b* — floor rotations for DS-2-1, DS-2-2, DS-2-3, and DS-2-4 (color should be used for this figure)

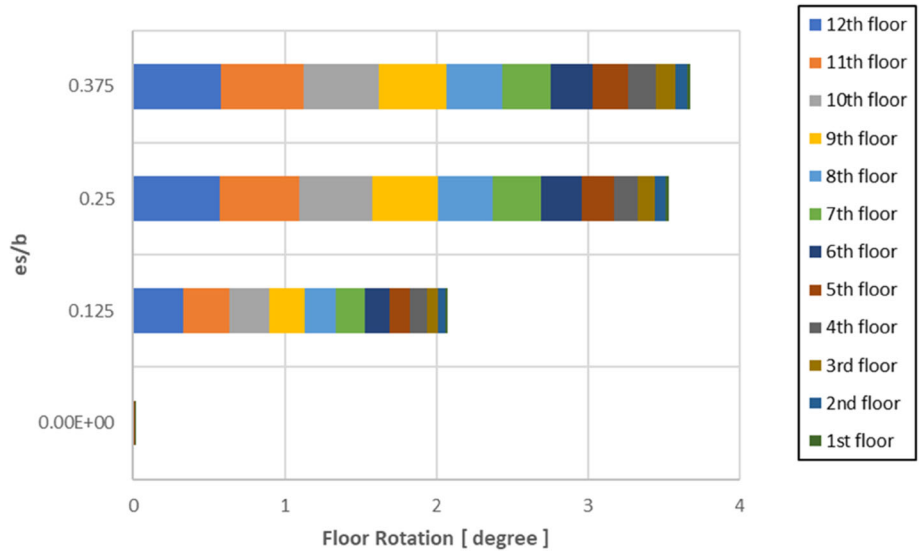

Figure 25: Comparison of *es/b* — floor rotations for DS-3-1, DS-3-2, DS-3-3, and DS-3-4 (color should be used for this figure)

for small eccentricity ratios and up to 42% for large eccentricity ratios. Only for the derived equation, there is no reduction in the design force ratio of stiff side elements for small and large eccentricity ratios.

Second group of buildings

The second group consists of five buildings are shown in Fig. 45. The five buildings have different eccentricity ratios. The buildings are 15-story in height, and the floor height is 3 m. The buildings have nine bays in *X*-direction and five in *Y*-direction. The building's structural system is dual with intermediate moment frames (without beams)

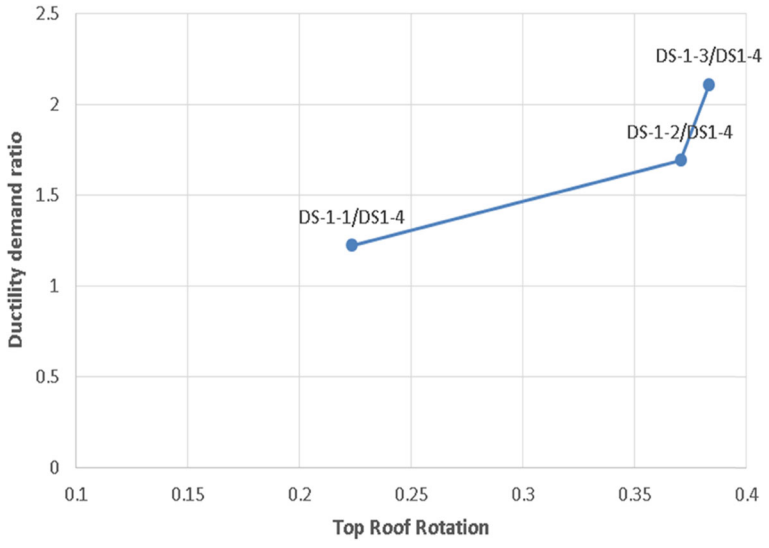

Fig. 26 Comparison of rotation — ductility demand the ratio for stiff elements located 16 m from center of mass for (DS-1-1, DS-1-2, and DS-1-3)

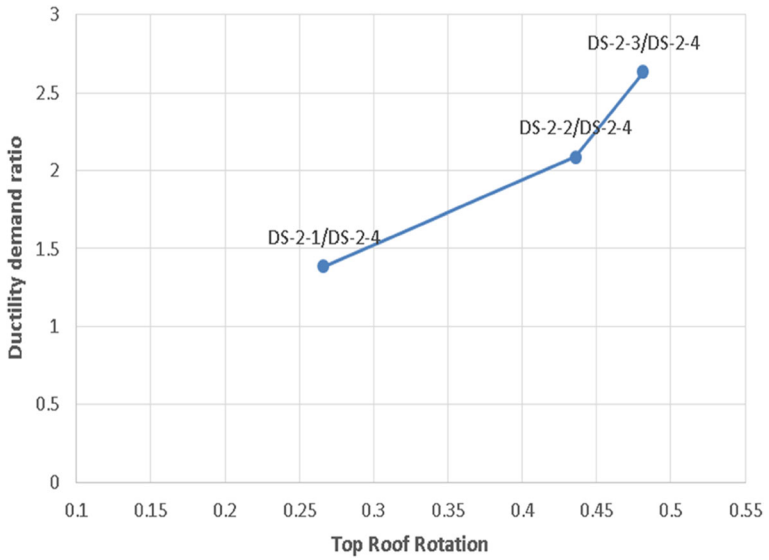

Fig. 27 Comparison of rotation — ductility demand ratio for stiff elements located 16 m from center of mass for (DS-2-1, DS-2-2, and DS-2-3)

and ordinary shear walls. Corner and edge columns are 300 * 1100 mm, and the other inner columns are 300 * 1400 mm. The concrete core consists of four walls, each wall length is 4 m, and the slab thickness is 160 mm. The columns are fixed at their base. The buildings were studied in *Y*-direction only.

First, the dimensions of the structural elements were determined by a preliminary design process using the equivalent static seismic load of ASCE 7-16. Second, the torsional irregularity was checked using various codes and the derived equations for all models, as shown in Tables 10, 11, 12, 13, and 14. Third, the torsional irregularity

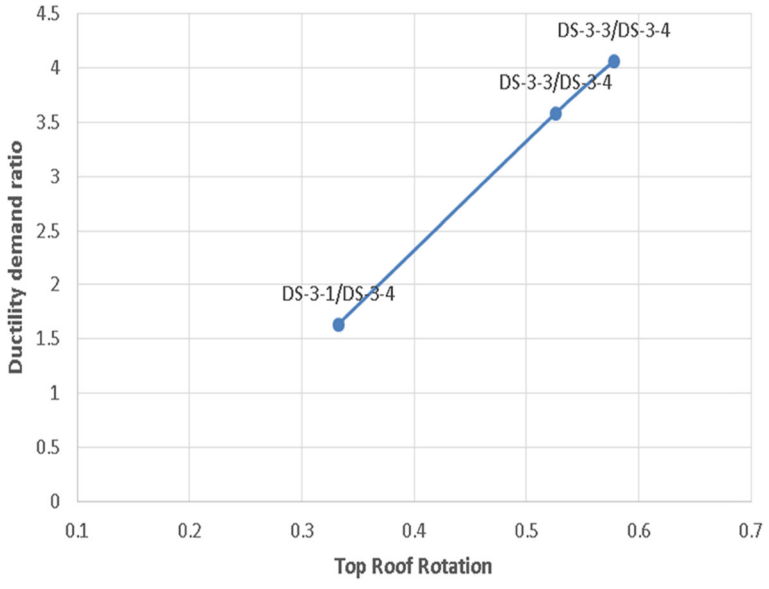

Fig. 28 Comparison of rotation — ductility demand the ratio for stiff elements located 16 m from center of mass for (DS-3-1, DS-3-2, and DS-3-3)

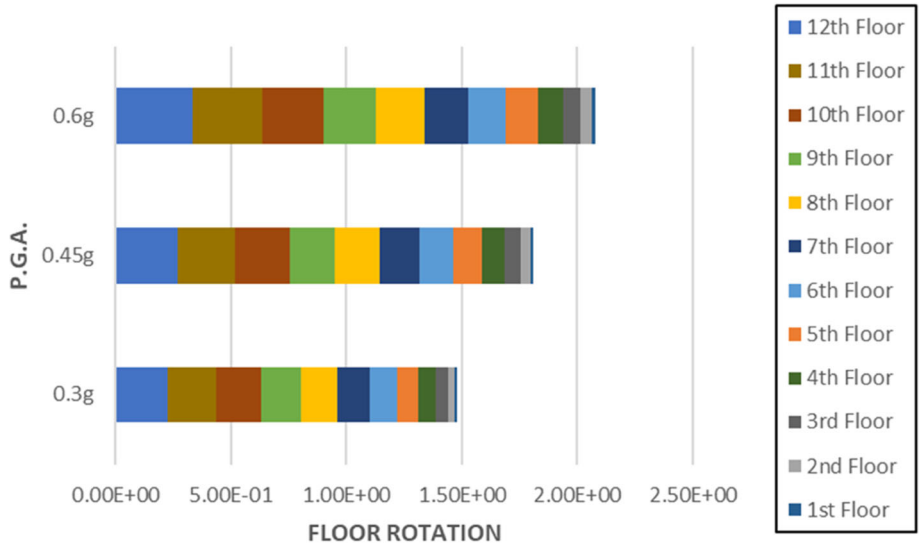

Fig. 29 Comparison of floor rotations — P.G.A. for (DS1-1, DS2-1, and DS3-1) (color should be used for this figure)

provisions of various codes and the derived equations were considered in the analysis. Fourth, the design forces of resisting elements of the asymmetric building correspond to those of symmetric building compared as shown in Figs. 46 and 47. Finally, the torsional amplification factor (A_x) of ASCE 7-16 and the derived equation are compared in Fig. 48.

Comparing the design forces of resisting elements of stiff side elements show that by neglecting the torsional irregularity provisions, there is a reduction in the design force up to 56% for small eccentricity ratios and up to 60% for large eccentricity ratios. For EC-8 code, there is a reduction in the design force ratio of stiff side elements up to 14% for small eccentricity ratios and up to 22% for large eccentricity ratios. For ASCE

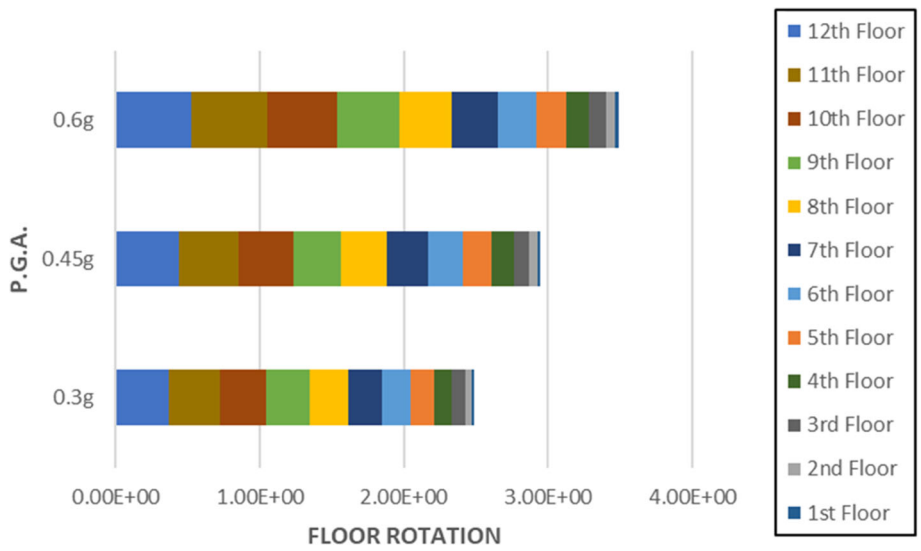

Fig. 30 Comparison of floor rotations — P.G.A. for (DS1-2, DS2-2, and DS3-2) (color should be used for this figure)

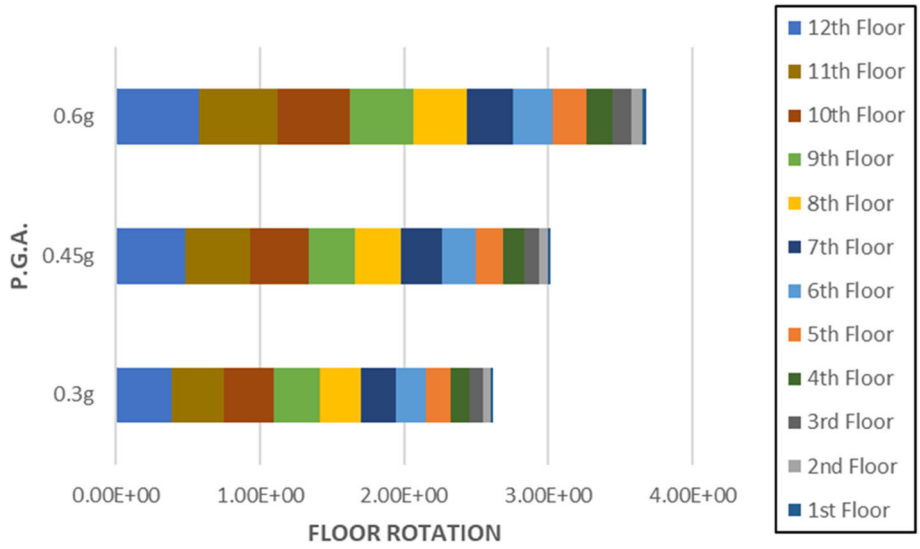

Fig. 31 Comparison of floor rotations — P.G.A. for (DS1-3, DS2-3, and DS3-3) (color should be used for this figure)

7-16, there is a reduction in the design force ratio of stiff side elements up to 44% for small eccentricity ratios and up to 52% for large eccentricity ratios. For Japanese code, there is a reduction in the design force ratio of stiff side elements up to 33% for small eccentricity ratios and up to 40% for large eccentricity ratios, only for derived equation, there is no reduction in the design force ratio of stiff side elements for small eccentricity ratios and a reduction in the design force ratio of stiff side elements up to 10% for large eccentricity ratios.

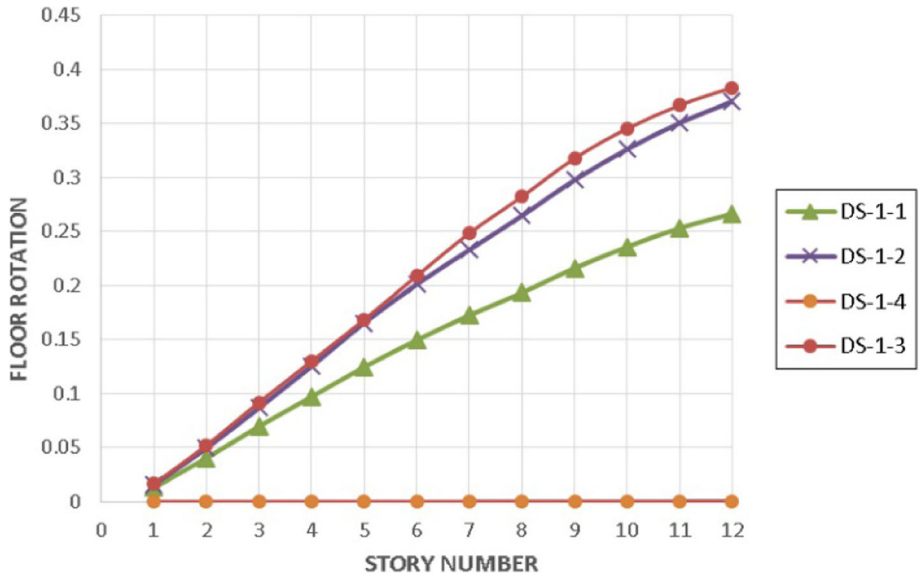

Fig. 32 Comparison of floor rotations — floor number for (DS-1-1, DS-1-2, DS-1-3, and DS-1-4)

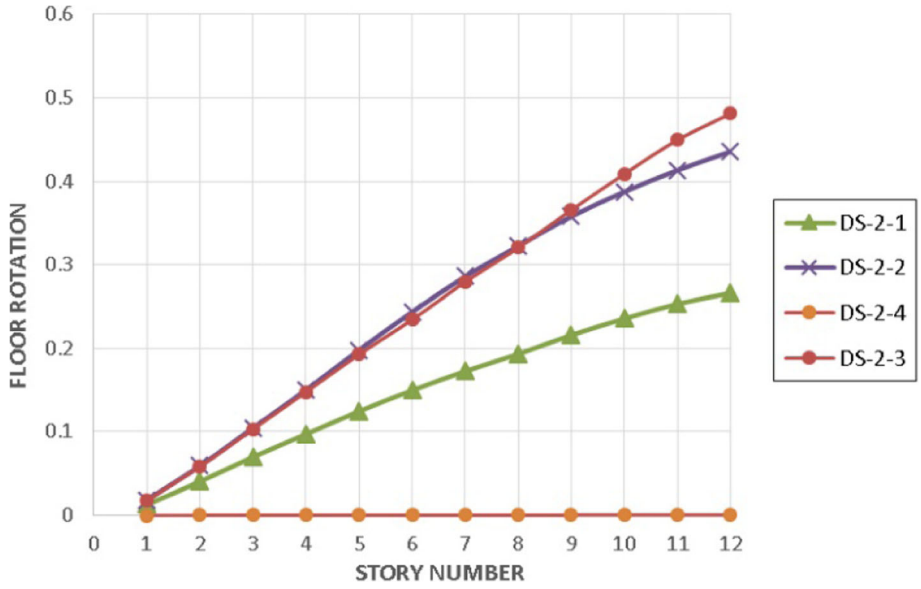

Fig. 33 Comparison of floor rotations — floor number for (DS-2-1, DS-2-2, DS-2-3, and DS-2-4)

Conclusions

This study performs a parametric investigation on Dual system buildings using nonlinear dynamic analysis to propose a new definition for torsional irregularity based on rigid floor rotations. Furthermore, two new equations were derived using nonlinear regression analysis based on these results. Finally, the torsional irregularity provisions of the proposed equations compared with the torsional irregularity provisions of Europe code (EC-8), Japanese code & ASCE 7-16 code, and the following points are concluded:

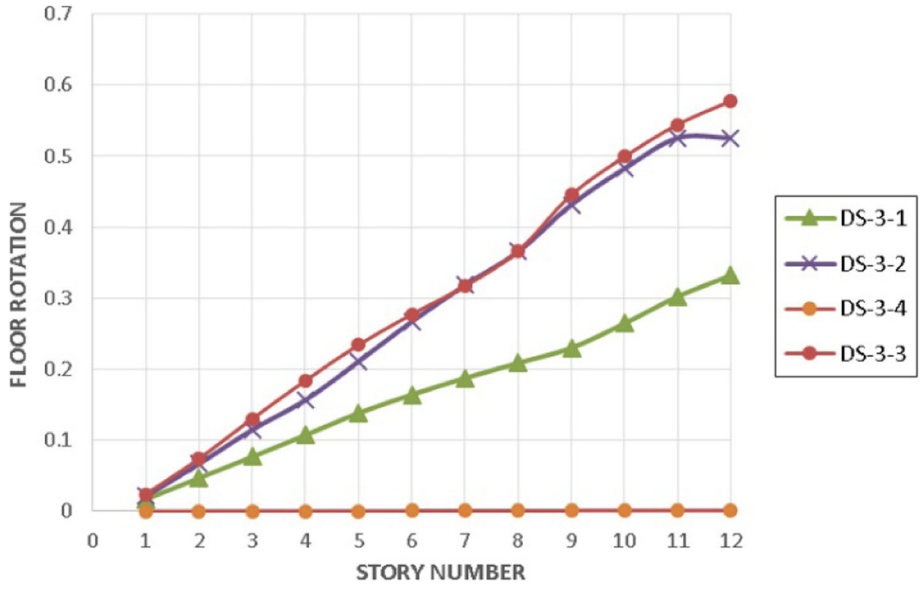

Fig. 34 Comparison of floor rotations — floor number for (DS-3-1, DS-3-2, and DS-3-3, and DS-3-4)

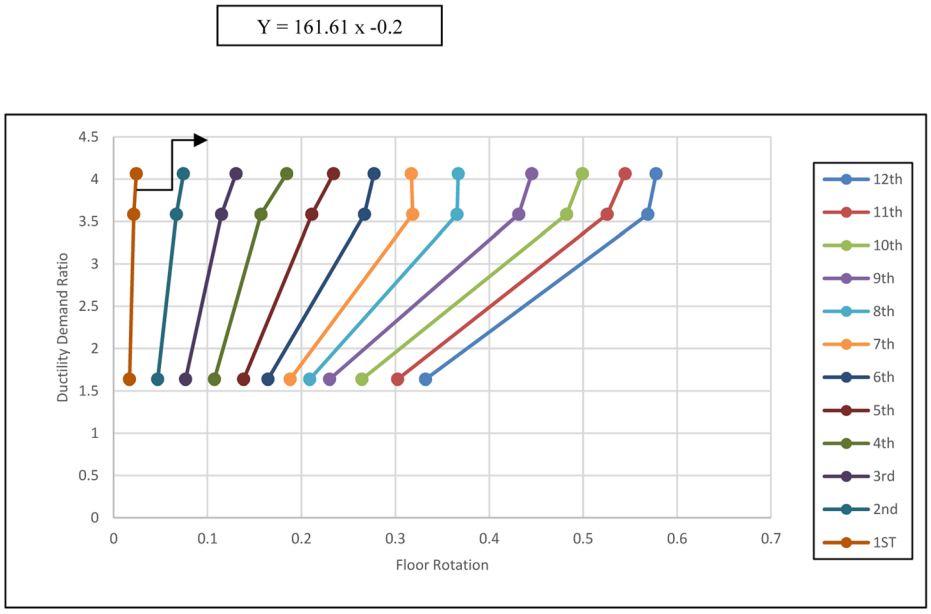

Fig. 35 Comparison of floor rotation — ductility demand ratio for stiff side elements located 16 m from center of mass for (DS-3-1, DS-3-2, and DS-3-3) (color should be used for this figure)

1. Comparing the results of the derived rotation-based equations to check the torsional irregularity with the results of the codes formula following points are concluded:

- The current form of the ASCE 7 code formula based on the maximum to average drift ratio gives that the torsional irregularity exists even if there is no eccentricity between the center of mass and the center of rigidity.

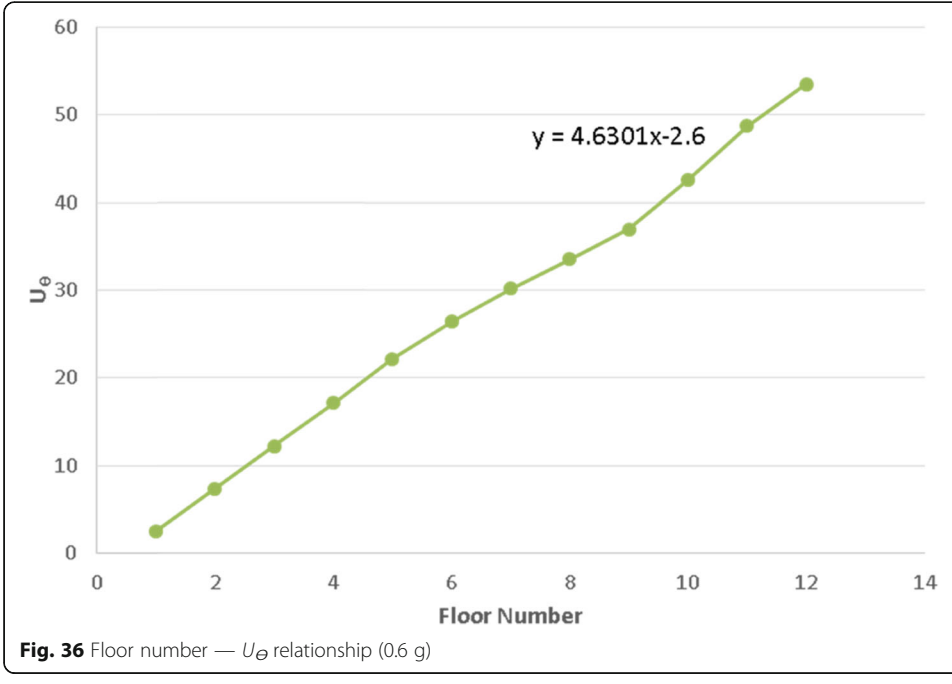

Fig. 36 Floor number — U_Θ relationship (0.6 g)

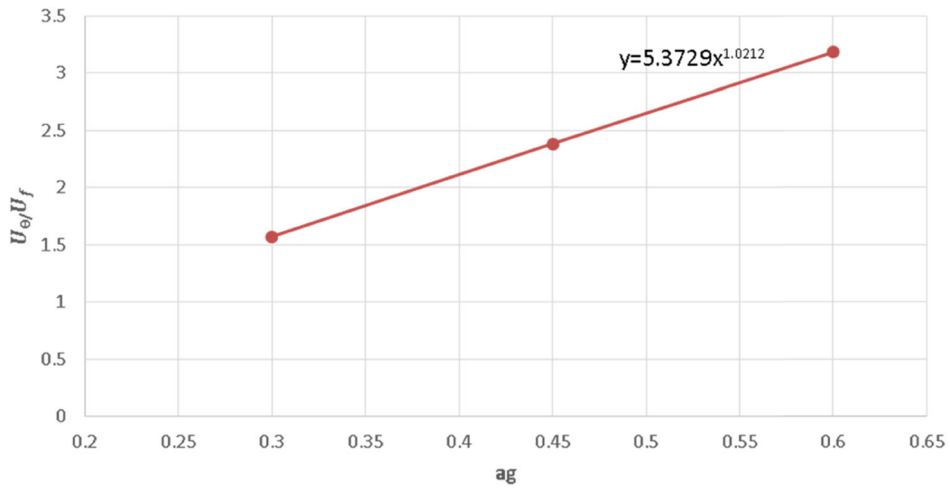

Fig 37 Ground acceleration (a_g) — $\frac{U\Theta}{Uf}$

- The current form of Japanese code formula based on the torsional radius gives in some cases that the torsional irregularity does not exist for eccentricity ratio (*es*/*b*) up to 0.15.
- The current EC-8 code formula based on the torsional radius & radius of gyration of the floor mass gives that torsional irregularity exists in all cases, even if the building is symmetric.
- For some cases where there is eccentricity between the center of mass and the center of rigidity, ASCE form gives that torsional irregularity does not exist for the upper floors of the building and exists in the lower floors.
- Only the rotation-based equation gives that the torsional irregularity does not exist if there is no eccentricity between the center of mass and center of rigidity which is more realistic.

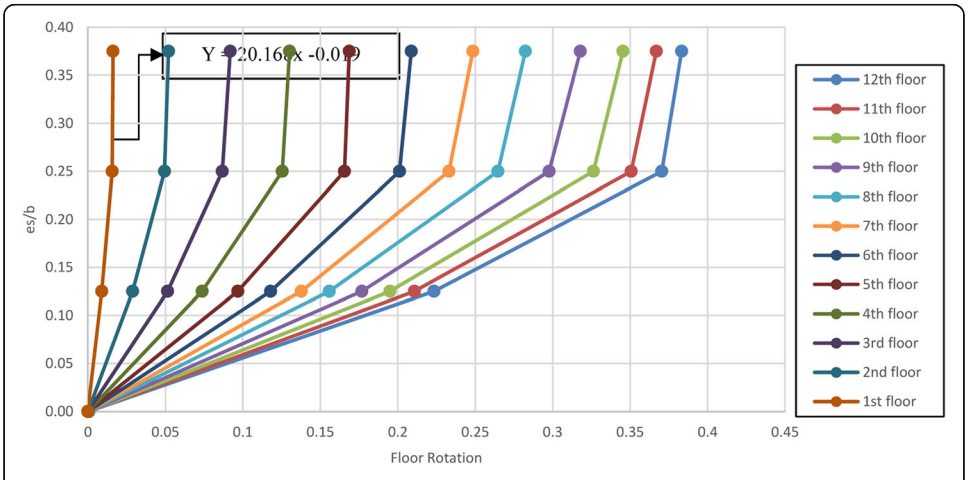

Fig. 38 Floor rotation — structural eccentricity normalized by plan dimension (*es*/*b*) relationship for Group-1 (0.3 g) (color should be used for this figure)

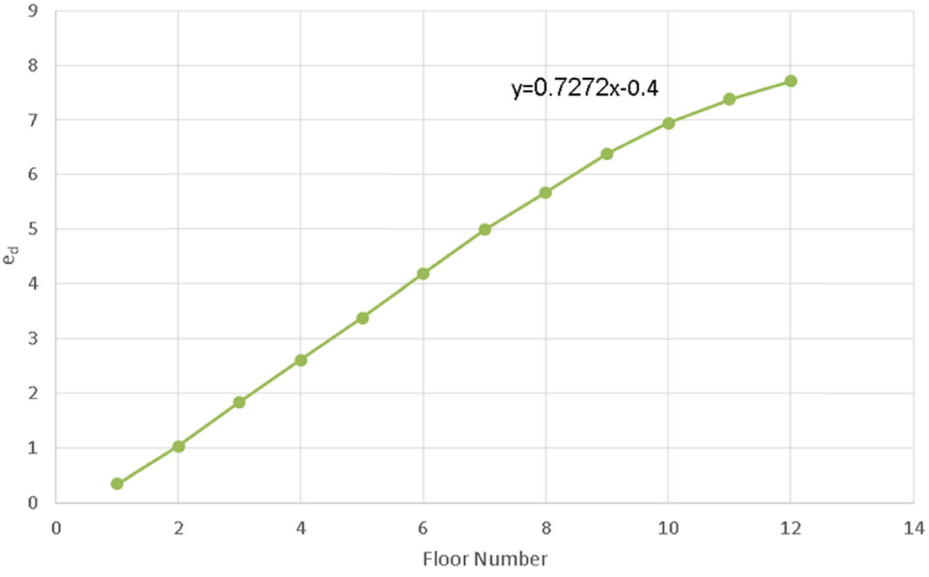

Fig. 39 Floor number — e_d relationship for Group-1 (0.3 g)

2. Comparing the results of the derived rotation-based equations of torsional irregularity coefficients with the results of the codes formula following points are concluded:

- The current form of the ASCE 7 code formula is based on the ratio of the maximum to average displacement; its torsional irregularity coefficients (A_x) reach maximum values when the structural walls are located as close as possible to the center of mass, and it decreases as eccentricities increase.

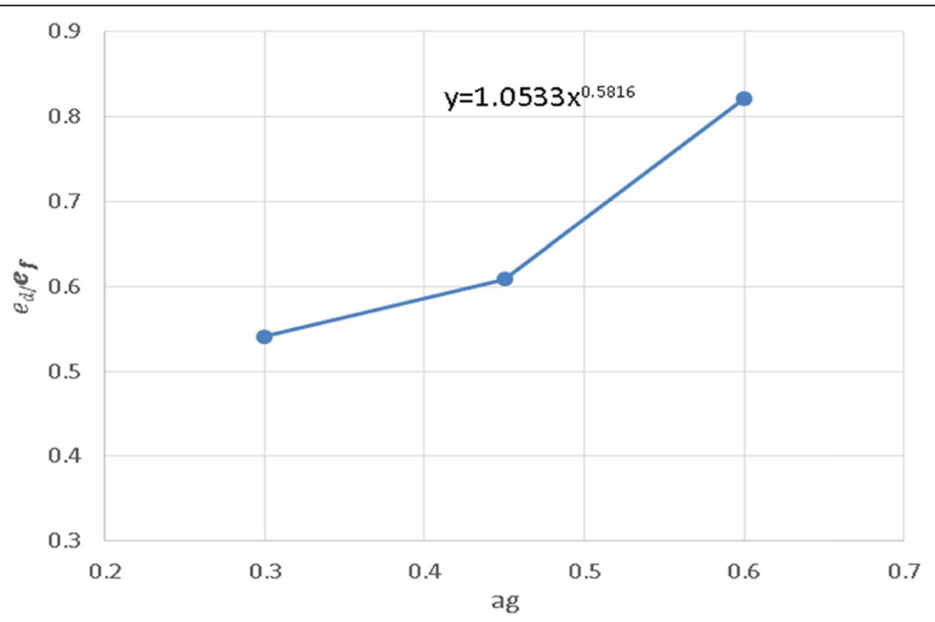

Fig. 40 P.G.A. — $\frac{e_d}{e_f}$ relationship

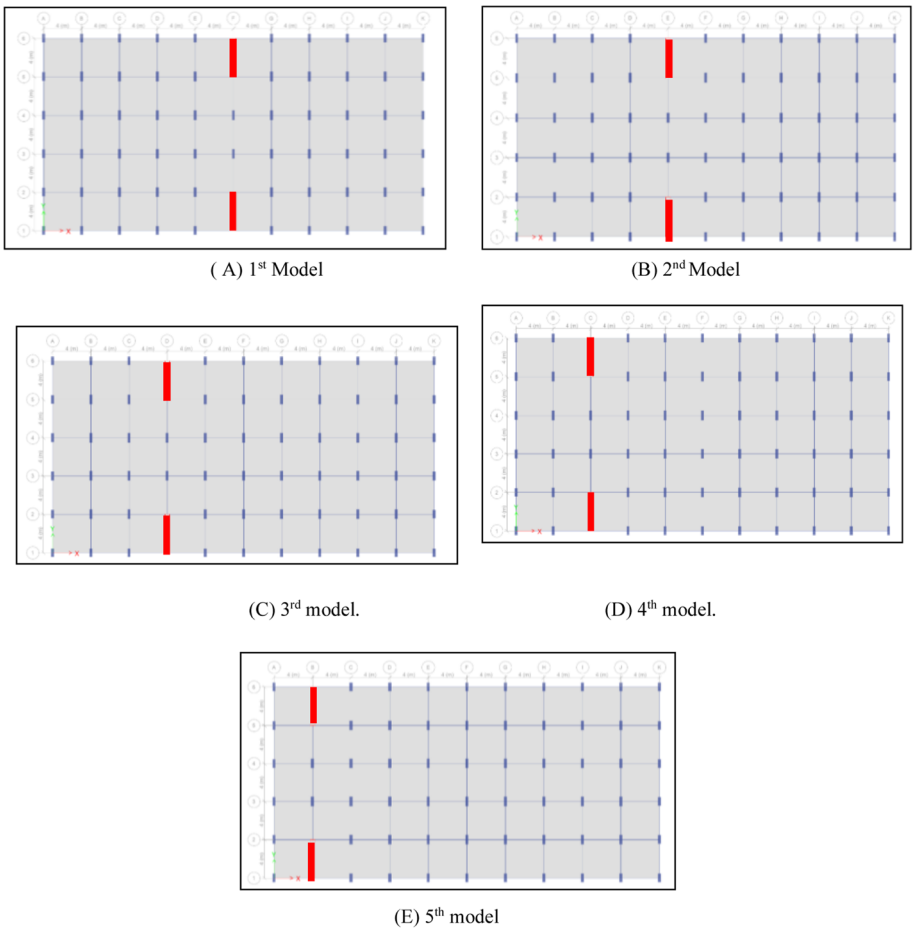

Fig. 41 First group models. **a** 1st Model. **b** 2nd Model. **c** 3rd model. **d** 4th model. **e** 5th model

Table 7 Torsional irregularity check of 1st model due to ASCE 7-16, EC-8, Japanese, and derived equation

Story	Load case	ASCE 7-16	Derived equation	EC-8	Japanese
11th to12th Floor	E.Q.Y+(0.05) eccentricity	No torsional irregularity	No torsional irregularity	Torsional irregularity	No torsional irregularity
1st to 10th Floor	E.Q.Y+(0.05) eccentricity	Torsional irregularity	No torsional irregularity	Torsional irregularity	No torsional irregularity

Table 8 Torsional irregularity check of 2nd and 3rd model due to ASCE 7-16, EC-8, Japanese, and derived equation

Story	Load case	ASCE 7-16	Derived equation	EC-8	Japanese
11th to12th Floor	E.Q.Y+(0.05) eccentricity	No torsional irregularity	Torsional irregularity	Torsional irregularity	No torsional irregularity
1st to10th Floor	E.Q.Y+(0.05) eccentricity	Torsional irregularity	Torsional irregularity	Torsional irregularity	No torsional irregularity

Table 9 Torsional irregularity check of 4th and 5th model due to ASCE 7-16, EC-8, Japanese, and derived equation

Story	Load case	ASCE 7-16	Derived equation	EC-8	Japanese
11th to 12th Floor	E.Q.Y+(0.05) eccentricity	No torsional irregularity	Torsional irregularity	Torsional irregularity	Torsional irregularity
1st to10th floor	E.Q.Y+(0.05) eccentricity	Torsional irregularity	Torsional irregularity	Torsional irregularity	Torsional irregularity

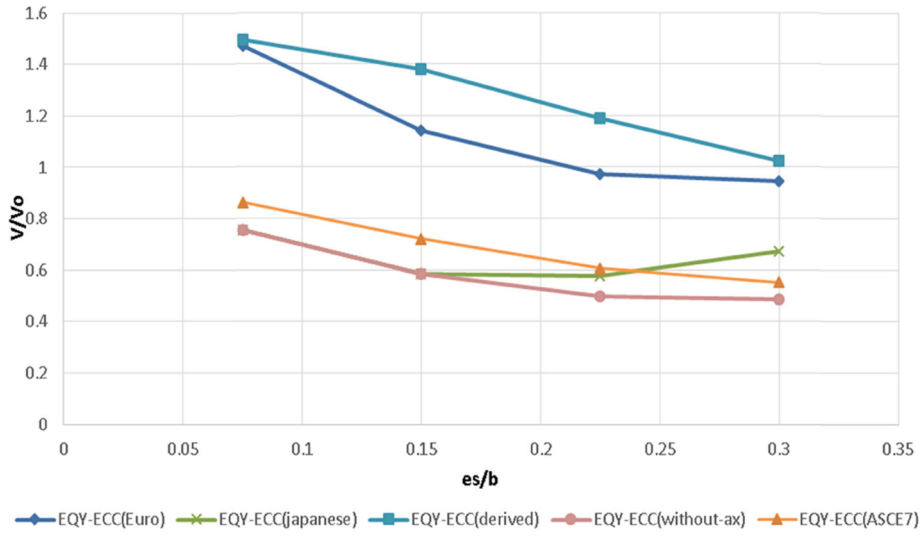

Fig. 42 Comparison of eccentricity ratio — design force ratio (design force in un-symmetric model V_o, normalized by design force in symmetric plan V) for stiff side elements for ASCE 7-16, EC-8, Japanese, derived equation, and without considering torsional irregularity

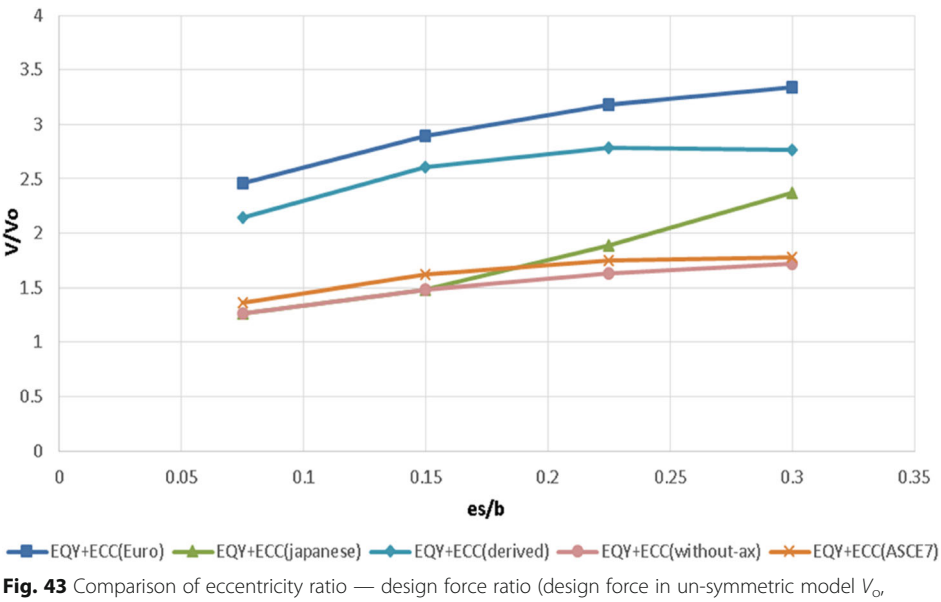

Fig. 43 Comparison of eccentricity ratio — design force ratio (design force in un-symmetric model V_o, normalized by Design Force in symmetric plan V) for flexible side elements for ASCE 7-16, EC-8, Japanese derived equation, and without considering torsional irregularity

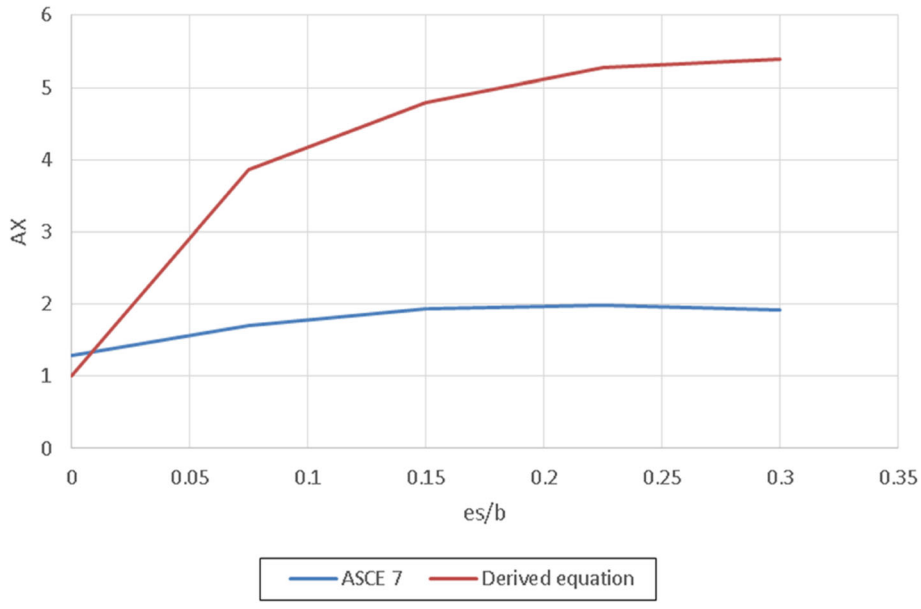

Fig. 44 Comparison of eccentricity ratio — max. A_x for ASCE 7-10 and derived equation

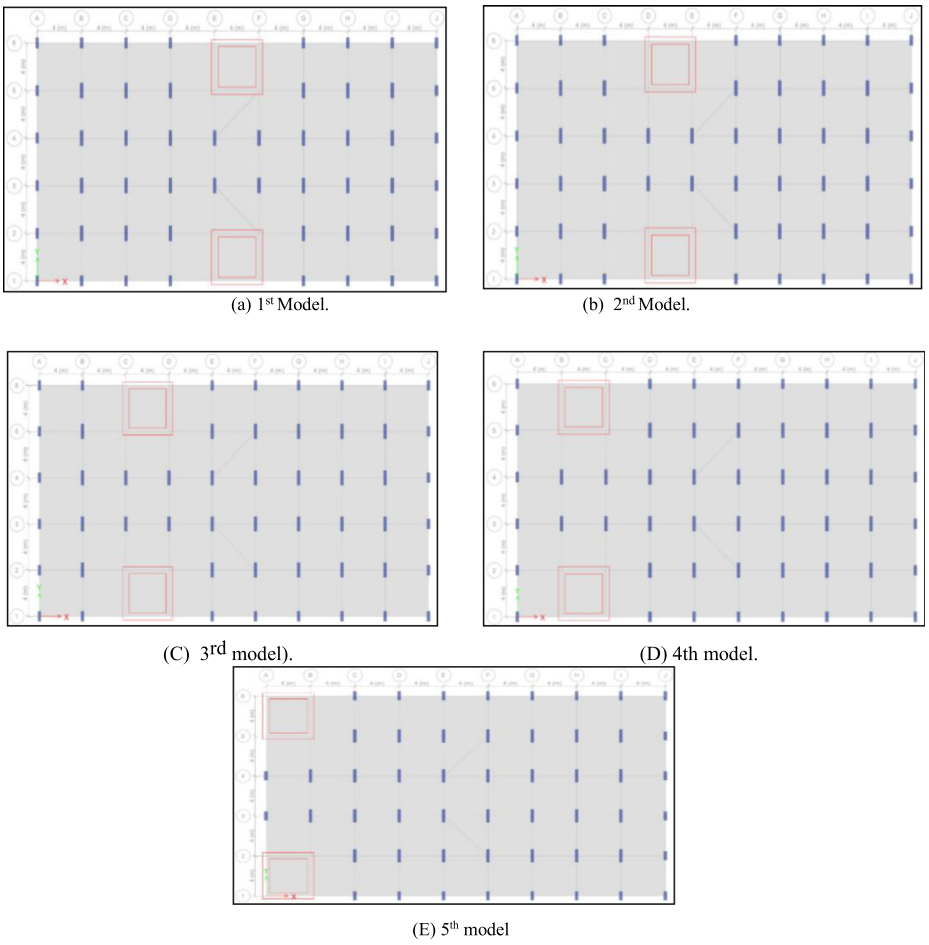

Fig. 45 Second group models. **a** 1st model. **b** 2nd model. **c** 3rd model). **d** 4th model. **e** 5th model

- Rotation-based equation gives torsional irregularity coefficients (A_x) increases as the distance between the center of mass and center of rigidity increases which is more realistic.

3. Comparing the results of the derived rotation-based equations of design forces of stiff side elements of un-symmetric system normalized symmetric system with the results of codes formulas, the results indicate that all the codes' torsional irregularity provisions are unconservative. Therefore, only the proposed equations provide an adequate estimate of the design force of the stiff side elements.

Table 10 Torsional irregularity check of 1st model due to ASCE 7-16, EC-8, Japanese, and derived equation

Story	Load case	ASCE 7-16	Derived equation	EC-8	Japanese
1st to 15th Floor	E.Q.Y+(0.05) eccentricity	No torsional irregularity	No torsional irregularity	Torsional irregularity	No torsional irregularity

Table 11 Torsional irregularity check of 2nd model due to ASCE 7-16, EC-8, Japanese, and derived equation

Story	Load case	ASCE 7-16	Derived equation	EC-8	Japanese
8th to15th Floor	E.Q.Y+(0.05) eccentricity	No torsional irregularity	Torsional irregularity	Torsional irregularity	Torsional irregularity
1st to 7th floor	E.Q.Y+(0.05) eccentricity	Torsional irregularity	Torsional irregularity	Torsional irregularity	Torsional irregularity

Table 12 Torsional irregularity check of 3rd model due to ASCE 7-16, EC-8, Japanese, and derived equation

Story	Load Case	ASCE 7-16	Derived equation	EC-8	Japanese
12th to15th Floor	E.Q.Y+ (0.05) eccentricity.	No torsional irregularity	Torsional irregularity	Torsional irregularity	Torsional irregularity
1st to11th floor	E.Q.Y+(0.05) eccentricity	Torsional irregularity	Torsional irregularity	Torsional irregularity	Torsional irregularity

Table 13 Torsional irregularity check of 4th model due to ASCE 7-16, EC-8, Japanese, and derived equation

Story	Load case	ASCE 7-16	Derived equation	EC-8	Japanese
15th Floor	E.Q.Y+(0.05) eccentricity	No torsional irregularity	Torsional irregularity	Torsional irregularity	Torsional irregularity
1st to 14th floor	E.Q.Y+(0.05) eccentricity	Torsional irregularity	Torsional irregularity	Torsional irregularity	Torsional irregularity

Table 14 Torsional irregularity check of 5th model due to ASCE 7-16, EC-8, Japanese, and derived equation

Story	Load case	ASCE 7-16	Derived equation	EC-8	Japanese
1st to 15th Floor	E.Q.Y+(0.05) eccentricity	Torsional irregularity	Torsional irregularity	Torsional irregularity	Torsional irregularity

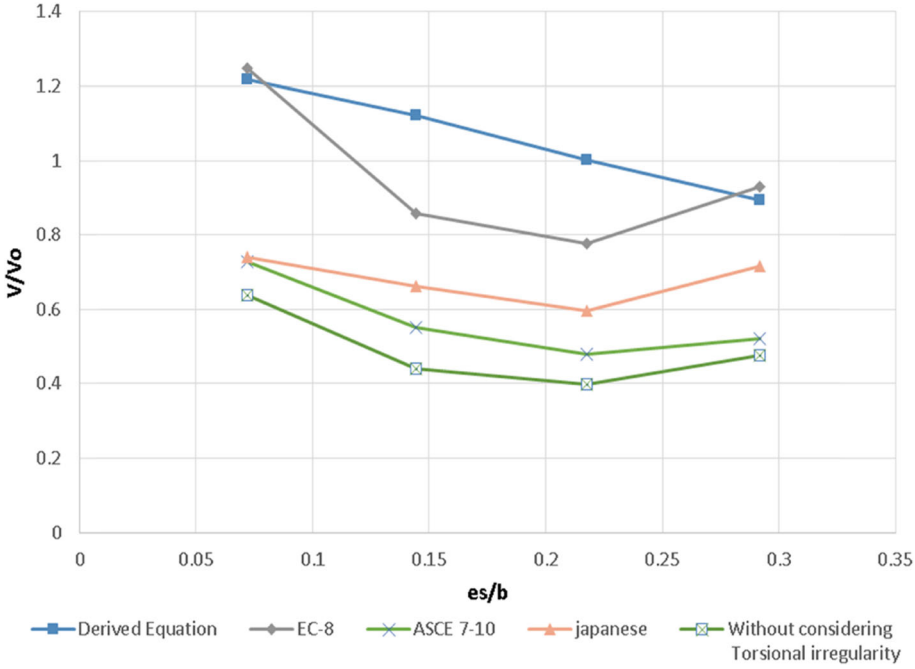

Fig. 46 Comparison of eccentricity ratio — design force ratio (design force in un-symmetric model V_o, normalized by design force in symmetric plan V) for stiff side elements for ASCE 7-10, EC-8, Japanese, derived equation, and without considering Torsional irregularity

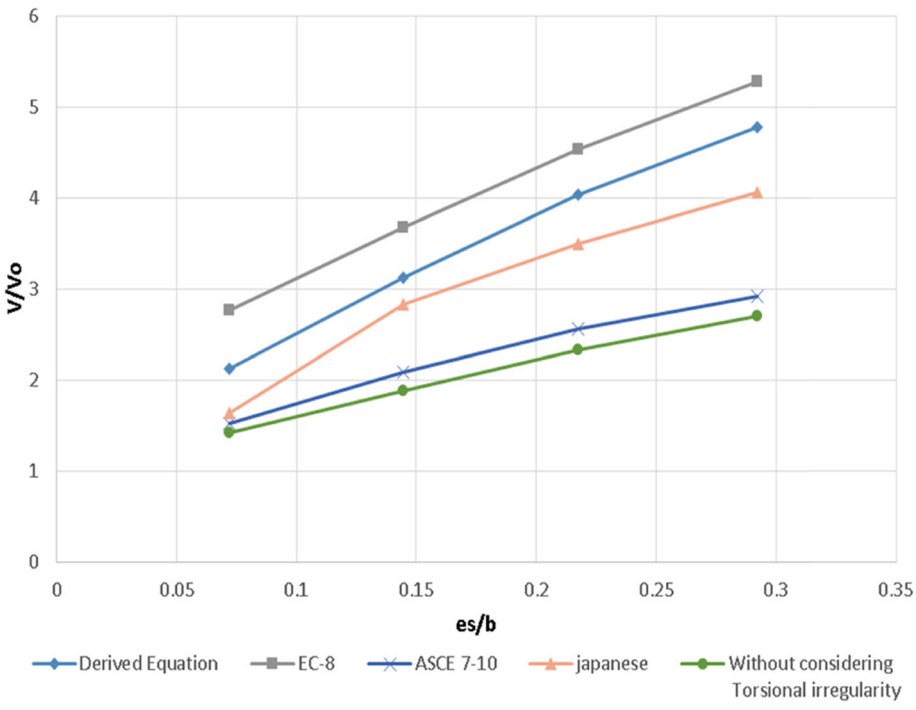

Fig. 47 Comparison of eccentricity ratio — design force ratio (design force in un-symmetric model V_o, normalized by design force in symmetric plan *V*) for flexible side elements for ASCE 7-10, EC-8, Japanese, derived equation, and without considering Torsional irregularity

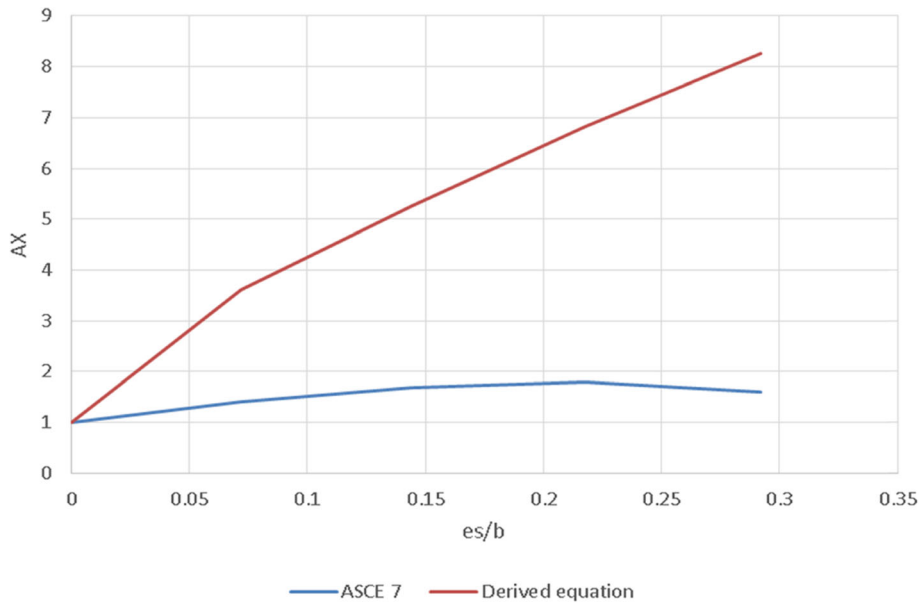

Fig. 48 Comparison of eccentricity ratio — max. A_x for ASCE 7-10 and derived equation

4. Comparing the results of the derived rotation-based equations of ratios of design forces for flexible side elements of un-symmetric system normalized symmetric system with the results of codes formula indicates that the flexible side elements provisions of all the studied codes are overly conservative.
5. Further studies are suggested to extend the proposed definition for other structural typologies of buildings, study the effects of plan asymmetry and its effect on eigenfrequency analysis, and propose an upper limit value for the torsional amplification factor for the flexible side elements for dual systems and other structural systems.

Abbreviations

α: Design eccentricity coefficient for flexible side elements; es: Distance between center of mass and center of rigidity; β: Accidental eccentricity coefficient; b: Plan dimension perpendicular to the direction of loading; δ: Design eccentricity coefficient for stiff side elements; δ_{max}: Maximum story displacement; δ_{avg}: Average story displacement; e_y: Plan eccentricity in the y-direction; I_x: Second moment of stiffness in the x-direction with respect to the center of rigidity; I_y: Second moment of stiffness in the y-direction with respect to the center of rigidity; K_x: Lateral stiffness in the x-direction; e_x: Plan eccentricity in the x-direction; K_y: Lateral stiffness in the y-direction; r_x: Torsional radius for x-direction; l_s: Radius of gyration of the floor mass; L: Plan dimension parallel to the direction of loading; R_y: Torsional radius for y-direction; a_u/a_1: Ratio of the multiplier of horizontal seismic design action at the formation of a global plastic mechanism to the multiplier of horizontal design seismic action at the formation of first plastic hinge in the system, which ranges from 1 to 1.3; $U^{\theta}{}_{o}$: Effect of rotation on ductility demand for the base case; U: Upper limit for the derived equation, if $U > 1$ torsional irregularity exists; U_f: The result of the division of floor number — U^{θ} relationship and $U^{\theta}{}_{or}$; U_g: The result of the division of $\frac{U^{\theta}}{U_f}$ — ground acceleration (a_g) relationship and $\frac{U^{\theta}{}_{o}}{U_f}$; $\boldsymbol{\Theta}$: Rigid floor rotations in degree; n: Floor number (e.g., 1 for 1st floor, 2 for 2nd floor, 3 for 3rd floor); $e_d{}^{o}$: Effect of rotation on the distance between the center of mass and the center of rigidity for the base case; e_f: The result of the division of floor number — e_d relationship and $e_d{}^{o}$; e_g: The result of the division of ground acceleration (a_g) — $\frac{e_d}{ef}$ relationship and $\frac{e_d{}^{o}}{ef}$; A_x: Torsional amplification factor

Acknowledgements
Not applicable.

Authors' contributions
K.M.A. designed the analyses, analyzed the data, and wrote the manuscript. The study was supervised and critically reviewed by K.F.E. and H.M.S. All authors read and approved the final manuscript.

Availability of data and materials
The datasets used and/or analyzed during the current study are available from the corresponding author on reasonable request.

Declarations

Competing interests

The authors declare that they have no competing interests.

Received: 16 August 2021 Accepted: 19 December 2021
Published online: 26 January 2022

References

1. Esteva L (1987) Earthquake engineering research and practice in Mexico after 1985 earthquake. Bull New Z Natl Soc Earthq Eng 20:159–200
2. Mitchell D, Tinawi R, Redwoo RG (1990) Damage to buildings due to 1989 Loma Prieta earthquake –A Canadian code perspective. Can J Civil Eng 17(5):813–834. https://doi.org/10.1139/l90-093
3. Mitchell D, DeVall RH, Saatcioglu M, Simpson R, Tinawi R, Tremblay R (1995) Damage to concrete structures due to the 1994 Northridge earthquake. Can J Civil Eng 22(5):361–377. https://doi.org/10.1016/0148-9062(96)87653-4
4. Bozorgnia Y, Tso WK (1986) Inelastic earthquake response of asymmetric structures.J. Struct Engrg 112(2):383–400. https://doi.org/10.1061/(ASCE)0733-9445(1986)112:2(383)
5. Chopra AK, Goel RK (1991) Effects of plan asymmetry in inelastic seismic response of one-story systems. J Struct Engrg 117(05):1492–1513. https://doi.org/10.1061/(ASCE)0733-9445(1991)117:5(1492)
6. Chopra AK, Goel RK (1991) Evaluation of torsional provisions in seismic codes. J Struct Engrg 117(12):3762–3782. https://doi.org/10.1061/(asce)0733-9445(1991)117:12(3762)
7. Rutenberg A, Eisenberger M, Sholet G (1992) Inelastic seismic response of code designed single storey asymmetry structures. J Engrg Struct 14(2):91–102. https://doi.org/10.1016/0141-0296(92)90035-O
8. Wong CM, Tso WK (1995) Evaluation of seismic torsional provisions in uniform building code. J Engrg Struct 121(10): 1436–1442. https://doi.org/10.1061/(ASCE)0733-9445(1995)121:10(1436)
9. Humar J, Kumar P (2000) A new look at the torsion design provisions in seismic building codes. In: Proceedings of the 12th World Conference on Earthquake Engineering, Auckland, New Zealand 1707:1-8.
10. Humar J, Kumar P (2004) Review of code provisions to account for earthquake induced torsion. In: Proceedings of the 13th World Conference on Earthquake Engineering, Vancouver, B.C., Canada 3220:1-6.
11. Valente M (2013) Seismic upgrading strategies for non-ductile plan-wise irregular R/C structures. Procedia Eng 54:539–553. https://doi.org/10.1016/j.proeng.2013.03.049
12. Ozmen G, Girgin K, Durgun Y (2014) Torsional irregularity in multi-story structures.Int J Adv. Struct Eng 6(4):121–131. https://doi.org/10.1007/s40091-014-0070-5
13. Valente M, Milani G (2018) Alternative retrofitting strategies to prevent the failure of an under-designed reinforced concrete frame. Eng Fail Anal 89:271–285. https://doi.org/10.1016/j.engfailanal.2018.02.001
14. American Society of Civil Engineers (2016), Minimum design loads and associated criteria for buildings and other structures. ASCE/SEI 7, Reston, VA.
15. U.B.C. (1997) Uniform building code, international conference of buildings officials, vol 97, Whittier, California, U.S.A
16. Teshigawara M (2012) Outline of Earthquake Provisions in the Japanese Building Codes. Architectural Institute of Japan (ed.). In: Preliminary Reconnaissance Report of the 2011 Tohoku-Chiho Taiheiyo-Oki Earthquake, Geotechnical, Geological and Earthquake Engineering, vol 23. Springer Japan, Tokyo, Japan
17. Eurocode-8 (2004), Design of structures for earthquake resistance. Part 1: General rules, seismic actions and rules for buildings, European Committee for Standardization; Brussels, Belgium.
18. Tagel-Din H, Meguro K (1999) Applied element simulation for collapse analysis of structures. Bull Earthq Resistant Struct Res Center 32:113–123
19. Meguro K, Tagel-Din H (2002) Applied element method used for large displacement structural analysis. J Nat Disaster Sci 24:25–34
20. Extreme loading for structures (ELS) (2018). http://www.appliedscienceint.com.
21. Maekawa K, Okamura H (1991) Nonlinear analysis and constitutive models of reinforced concrete. Tokyo, Gihodo Shuppan
22. Meguro K, Tagel-Din H (2001) Applied element simulation of R.C. structure sunder cyclic loading. J Engrg Struct 127(11): 1295–1305. https://doi.org/10.1061/(asce)0733-9445(2001)127:11(1295)
23. Menegotto M, Pinto PE (1973, 1973) Method of analysis for cyclically loaded reinforced concrete plane frames including changes in geometry and non-elastic behavior of elements under combined normal force and bending. In: Proceedings of IABSE Symposium on Resistance and Ultimate Deformability of Structures Acted on by Well Defined Repeated Loads, International Association of Bridge and Structural Engineering, Lisbon, Portugal, 1973;13: 15-22.
24. Karbassi A, Nollet M-J (2013) Performance-based seismic vulnerability evaluation of masonry buildings using applied element method in a nonlinear dynamic-based analytical procedure. Earthq Spectra 29:399–426
25. Malomo D, Pinho R, Penna A (2020) Applied element modelling of the dynamic response of a full-scale clay brick masonry building specimen with flexible diaphragms. Int J Archit Herit 14:1484–1501.
26. Sediek O.A., El-Tawil S ; McCormick (2021), J. Seismic debris field for collapsed RC moment resisting frame buildings. J Struct Eng 147, 04021045.
27. ETABS (2016). http://www.csiamerica.com.
28. ACI Committee 318 (2014), Building code requirements for structural concrete and commentary (ACI 318-14),American Concrete Institute, Farmington Hills, MI.
29. Seismosoft Ltd (2016). SeismoArtif's help system. http://www.seismosoft.com/support/seismoartif-support/.
30. Park R (1988) Ductility evaluation from laboratory and analytical testing Proceedings of the 9th World Conference on earthquake Engineering, Tokyo, Japan 3:605-61.

Publisher's Note